EXAMENSARBETE INOM KEMITEKNIK,
AVANCERAD NIVÅ, 30 HP
STOCKHOLM, *SVERIGE 2021*

Modeling and optimisation of a rotary kiln reactor for the processing of battery materials

DANIAL KHAWAJA

KTH
SKOLAN FÖR KEMI, BIOTEKNOLOGI OCH HÄLSA

TRITA CBH-GRU-2021:199

Sammanfattning

Roterugnar är cylindriska kärl som används för att höja materials temperaturer i en kontinuerlig process som kallas för kalcinering. Roterugnar kan tillämpas i olika processer såsom reduktion av oxidmalm samt återvinning av farligt avfall. Fördelen med roterugnar ligger i dess förmåga att hantera råmaterial som sträcker sig från slam till granulära material med en mängd olika partikelstorlekar, och därigenom upprätthålla distinkta miljöer såsom en bädd av fasta partiklar som samexisterar med ett oxiderande fribord. Sex olika bäddbeteende har dokumenterats med avseende på fyllningsgrad samt Froude nummer. Syftet med denna studie var att utveckla en tvådimensionell suspensions modell med CFD genom att använda den kommersiella mjukvaran COMSOL 5.5 för att simulera de två faser, gas och fast, som en blandad fas efter verk av Philips et. al., Physics of Fluids A: Fluid Dynamics 4.1 (1992) 30-40 och Acrivos & Zhang., International Journal Multiphase Flow 20.3 (1994) 579-591. Denna modell undersöktes genom att jämföra den med de dokumenterade flödesregimerna samt genom parameter som partikelstorlek, partikeldensitet och viskositeten hos gas i flödesregimen känd som rullande läge. Dessutom undersöktes temperaturprofilen för den roterande ugnen genom att utforska hur blandningsvariationer av den fasta bädden i den roterande ugnen påverkas av värmeöverföringen när värme tillförs från väggen under rullande läge.

Resultaten av den tvådimensionella suspension modellen visade att det var bara möjligt att simulera glidläge korrekt; andra lägen kunde inte beskrivas som dokumenterat i litteraturen. Det indikeras att vilovinkeln och viskösa krafter i den roterande ugnen var låga vilket resulterade i att suspensions modellen inte kunde avbilda exakt de återstående flödesregimerna som dokumenterat. Till exempel avbildades rullningsläget mer likt forsandeläge då partiklarna fall fritt efter höjning av bädden. Partikelstorlek och partikeldensitet har visat sig ha en betydande påverkan på suspensions modellen eftersom de viskösa krafterna blir låga för en partikelstorlek och partikeldensitet under 0,4 mm respektive 1500 kg/m^3. Angående gasens viskositet visades det sig att ju närmare värdet 2.055e-3 (Pa*s) den blev desto större blev sedimentationsflödet vilket resulterade i att bäddpar-

tiklarna dras ner och förblir där. Suspensions modellen kunde således simulera en fast och flytande fas och inte en gasfas som avsett. Slutligen visade temperaturanalysen att påverkan av den termiska konduktiviteten var mer signifikant än den specifika värmekapaciteten i intervallet 1 - 50 (W/(m*K)) respektive 300 - 800 (J/(kg*K)) på grund av den tid det tog att nå en homogen temperaturprofil.

Abstract

Rotary kilns are cylindrical vessels used to raise materials temperature in a continuous process known as calcination. Rotary kilns find application in various processes such as reduction of oxide ore and hazardous waste reclamation. The advantage of the rotary kiln lies in its ability to handle feedstock ranging from slurries to granular materials with a variety of particle size, thereby maintaining distinct environments such as a bed of solid particles coexisting with an oxidising freeboard. Six different bed behaviours within the kiln have been documented with respect to the filling degree and Froude number. The aim of this study was to develop a two-dimensional suspension model with CFD by using the commercial software COMSOL 5.5 to simulate the two phases, gas and solid, as a mixed phase, following the works of Philips et. al., Physics of Fluids A: Fluid Dynamics 4.1 (1992) 30-40 and Acrivos & Zhang., International Journal Multiphase Flow 20.3 (1994) 579-591. This model was investigated by comparing it against the documented flow regimes as well as through parameters such as particle size, particle density and viscosity of gas in the flow regime known as rolling mode. In addition, the temperature profile of the rotary kiln was investigated by exploring how the mixture variation of the solid bed within the rotary kiln affects the heat transfer when heat is supplied from the wall during a rolling mode.
The results of the two-dimensional suspension model showed that it was only possible to simulate the slipping mode accurately; others mode could not be described as documented in literature. It is indicated that the angle of repose and viscous forces within the rotary kiln were low resulting in the suspension model not being able to accurately depict the remaining flow regimes as documented. For instance, the rolling mode was depicted more as a cataracting mode due to the free fall of particles after elevation of the bed. The particle size and the particle density were found to have a significant impact on the suspension model as the viscous forces became low for a particle size and particle density below 0.4 mm and 1500 kg/m^3 respectively. As for the viscosity of gas it was found that the closer it got to the value 2.055e-3 (Pa*s) the sedimentation flux became too large resulting in the bed particles being pulled down and remaining there. Thus, the suspension model could simulate a solid and liquid phase and not a gas

phase as intended. Lastly, the temperature analysis revealed that the impact of the thermal conductivity was more significant than the specific heat capacity in the range of 1 - 50 (W/(m*K)) and 300 - 800 (J/(kg*K)) respectively, due to the time it took to reach a homogeneous temperature profile.

Acknowledgements

This study is dedicated to my family who have been supporting me throughout my time at KTH and in life by teaching me to beocme a better person. Without you I would have never become the person I am today. Only through your encouragement and support have I been able to make it this far in life. There are no words to express how much I appreciate what you have done for me so far and continue to do. I will always remain grateful to you and will do my best to live up to your expectations.

I thank my supervisor Ramiar Sadegh-Vaziri for giving me the opportunity to work with this study. I am thankful for the honesty, support, patience, and guidance you have given me throughout the study. The lessons you have given me throughout the study are lessons I will take with me on my next chapter in life. I also give thanks to my examiner Matthäus Bäbler for being able to help me as well during my study by making time for me to answer all of my questions.

Nomenclature

ω	Rotation speed (1/s)
h_m	Hydraulic mean depth (m)
g	Acceleration of gravity (m/s^2)
μ	Mixture viscosity (Pa*s)
D	Diffusivity (m/s^2)
μ_c	Pure solvent viscosity (Pa*s)
ϕ_s	Solid concentration (-)
ϕ_{max}	Maximum solid concentration (-)
$\dot{\gamma}$	Rate-of-strain tensor (1/s)
v	Velocity (m/s)
p	Pressure (Pa)
K_c	Experimentally determined coefficient for spatially varying interaction frequency (-)
N_c	Spatially varying interaction frequency flux (m/s)
K_μ	Experimentally determined coefficient for spatially varying viscosity (-)
N_μ	Spatially varying viscosity flux (m/s)
N_g	Sedimentation flux (m/s)
ρ	Effective density (kg/m^3)
ϵ	Reduced density difference (-)

ρ_c	Pure solvent density (kg/m^3)
ρ_s	Pure solid density (kg/m^3)
u_{st}	Stokes settling velocity (m/s)
$f(\phi_s)$	Hindrance function (-)
N_S	The total flux of a particle (m/s)
L	Characteristic length (m)
N_b	Brownian diffusion flux(m/s)
j	Volume-averaged mixture velocity (m/s)
j_{slip}	The slip flux (m/s)
u_{slip}	Relative velocity between two phases (m/s)
u_s	Solid phase velocity (m/s)
j_{xx}	Gradient of velocity mixture jx, x-component (1/(s))
j_{xy}	Gradient of velocity mixture jx, y-component (1/(s))
j_{yx}	Gradient of velocity mixture jy, x-component (1/(s))
j_{yy}	Gradient of velocity mixture jy, y-component (1/(s))
i	solid or solvent phase
$C_{p,i}$	Specific heat capacity of phase i (J/(kg*K))
q_i	Heat flux of phase i (J/(m^2*K))
k_i	Thermal conductivity of phase i (W/(m*K))
θ	Dimensionless parameter for temperature profile (-)
a	Particle radius (m)
$T_{s,min}(t)$	The minimum temperature of the solid phase at a given time (K)
$T_{s,0}$	The initial temperature of the solid phase (K)
T_w	The max temperature given from the wall (K)
k_s	Thermal conductivity of the solid phase (W/(m*K))

$C_{p,s}$ Specific heat capacity of the solid phase (J/(kg*K))

k_g Thermal conductivity of the gas phase (W/(m*K))

$C_{p,g}$ Specific heat capacity of the gas phase (J/(kg*K))

$T_{g,0}$ The initial gas temperature (K)

Contents

List of Figures

List of Tables

Chapter 1

Introduction

In this section an introduction to rotary kilns will be given. In addition, the purpose of this master thesis will be given.

1.1 Rotary kiln

Rotary kilns are cylindrical vessels that are slightly inclined horizontally and that slowly rotated about their longitudinal axis. They can be found in material processing operations such as reduction of oxide ore, reclamation of hydrate lime and hazardous waste reclamation. The reason for the wide range of usage is due to the rotary kiln abilities such as being able to handle various feedstock from slurries to granular materials with large variations in particle size along with their ability to maintain distinct environments such as bed coexisting with an oxidising freeboard. Rotary kilns allow for residence times of the order of 2-5 s and temperatures as high as 2000 K which makes them a competitive operation device. However, the operation of a rotary kiln is not without any issues. These issues range from dust generation, low thermal efficiency and nonuniform product quality. Various methods can be used to combat mentioned issues for instance for the nonuniform product quality a longer residence time (usually longer than one hour) can be implemented to ensure higher uniformity. Essentially, rotary kilns are heat exchangers where the energy from a hot gas phase is extracted by the bed material and the bed material undergoes various heat exchange processes along the rotary kiln. A typical sequence for heat exchange in rotary kiln would be drying, heating, and chemical reaction over a wide range of temperature. Rotary kilns may also have external heating as well, but this is usually seen in special cases. A common configuration of the flow inside of a rotary kiln is shown in figure 1.1.1 which shows a counter-current flow[1].

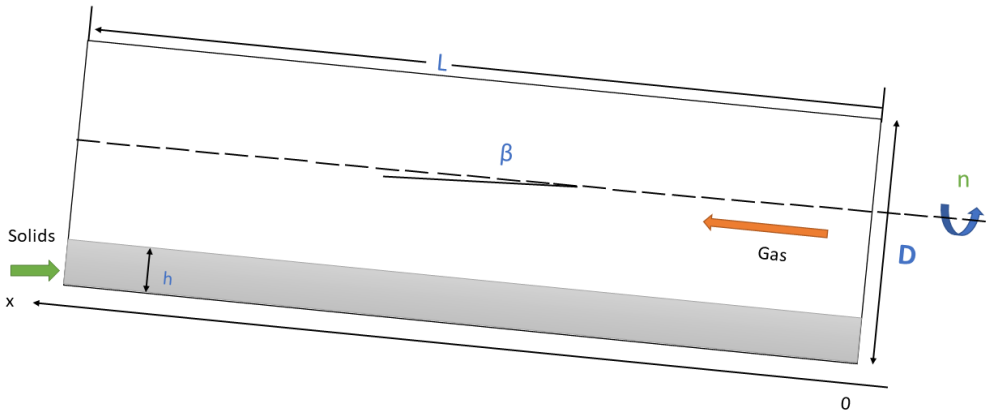

Figure 1.1.1: A typical counter-current configuration of a rotary kiln.

1.2 Rotary kiln design

Rotary kilns can be used for heating, reacting, and drying of solid materials and most of the time it is a combination of these three processes. The heat transfer, flow of material through the rotary kiln, gas-solid mass transfer and chemical reaction are the four aspects to consider when designing the rotary kiln. Of these four aspects the heat transfer plays an important role as this will determine the performance of the rotary kiln due to the heat transfer limiting the performance of the rotary kiln[2].

One can consider a radial cross-section through a rotary kiln as shown in figure 1.2.1. What is shown is the movement of particles within the bed of a rotary kiln due to rotating from the rotary kiln walls. This bed has two distinctive regions, the region near the free surface is called the active layer and a passive layer that is below. Through rotation of the rotary kiln, the particles in the passive layer will move along the walls of the rotary kiln until it reaches the surface of the bed and slides downwards into the active layer. These processes can be considered to be repeating for the particles. This may cause the particles to move in an axial direction when the rotary kiln is tilted in the axial direction when moving down in the active layer. It is from this that the models to predict the bed fill along the rotary kiln as a function of solids feed rate can be performed. In the rotary kiln, gas may flow through the freeboard region of the rotary kiln either

co—currently or counter-currently to the solid particles in the rotary kiln. Thus, it is to be expected that a different set of conditions apply to the solid and the gas at any point along the rotary kiln[2].

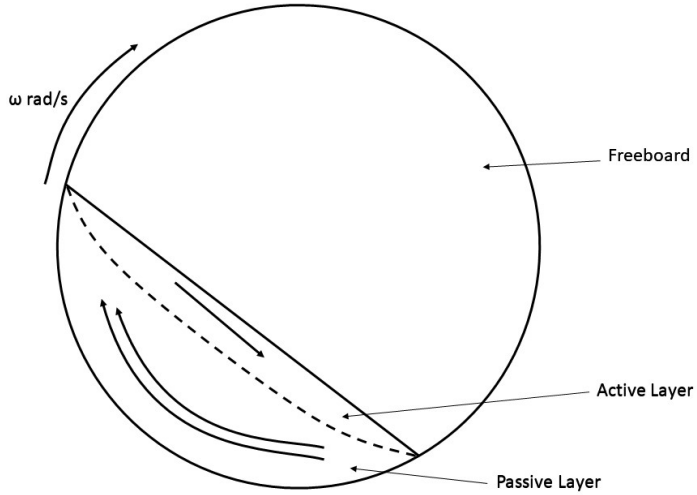

Figure 1.2.1: Radial cross section of a rotary kiln showing the active layer, passive layer and freeboard.

1.3 Bed behaviour diagram

The flow of the solid particles in the rotary kiln has been found to change significantly depending on particle characteristics, kiln size, rotation speed and bed fill. The Bed Behaviour Diagram is a concept that is intended to explain the different characteristics motion for the bed at different filling degrees as seen in figure 1.3.1. This diagram uses the Froude number shown in eq 1.3.1 to illustrate the change of mode with respect to filling degree. The filling degree describes the volumetric filling percentage of material inside the kiln. The Froude number is a dimensionless number which explains the ratio of inertia force on an element to the weight of the fluid element. In this case, it will be the ratio of centrifugal forces to the gravitational force[3]. It is of expressed as followed:

$$Fr = \frac{\omega^2 h_m}{g} \tag{1.3.1}$$

where ω is the rotation speed (1/s), h_m the hydraulic mean depth (m) and g the acceleration of gravity (m/s^2).

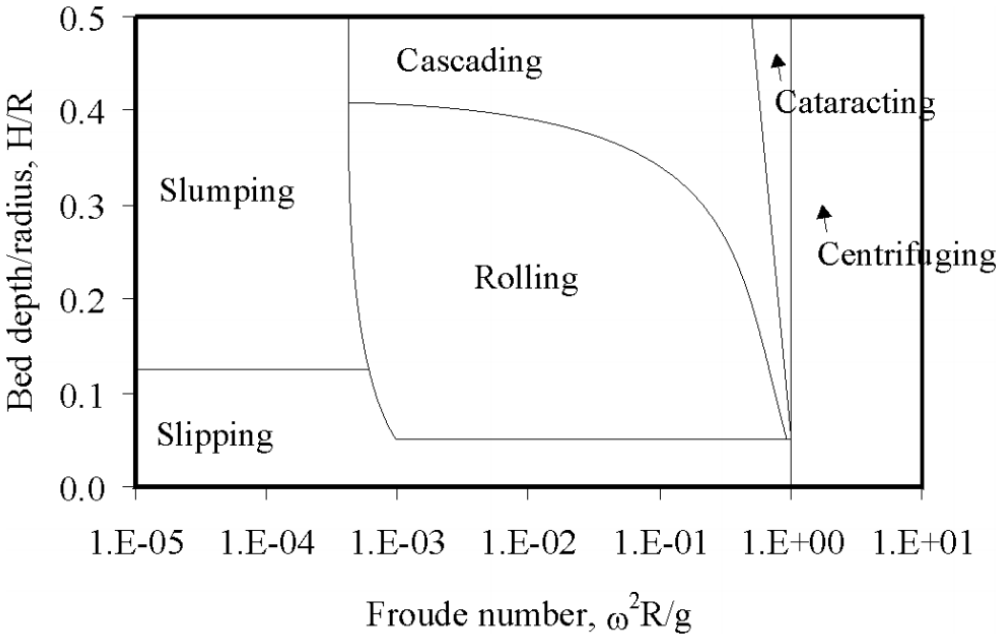

Figure 1.3.1: Bed Behaviour Diagram of a Rotary kiln[3].

There are six different zones seen in figure 1.3.1 that include different bed behaviour modes, the latter are shown visually in figure 1.3.2. These modes describe the particle movement due to the rotation. The first mode known as the slipping mode, is characterised by very small particle movement and an active layer that is very thick compared to the passive layer. The second mode, known as slumping occurs at a higher filling degree and is characterised when particles are elevated through movement along the wall, but then they will suddenly collapse and fall down to their initial position. The rolling mode, is the most desirable mode. Here the particles are renewed throughout the process itself and a dominant active layer can be seen, resulting in increased mixing, mass transfer and heat transfer due to the circular movement of the bed. Increasing the filling degree here near the rolling mode will result into the cascading mode a typical characterisation of the cataracting mode is that it is hard to distinguish between the active and passive layer. This is due to the particles showing a strong accumulation on the elevated side as well as on the top layer of the particle bed. The last two modes, cataracting, and centrifuging occur at high rotational speeds. In the cataracting mode, an improved mixing with the bed and freeboard is achieved as the particles will now fall free after reaching a certain elevation. However, as seen in figure 1.3.1 this operational range is very small and it is therefore not optimal for operation. Lastly, the centrifuging mode results in a dominant active

layer with poor mixing and poor heat transfer as the particles are pressed to the walls due to the centrifugal forces [4].

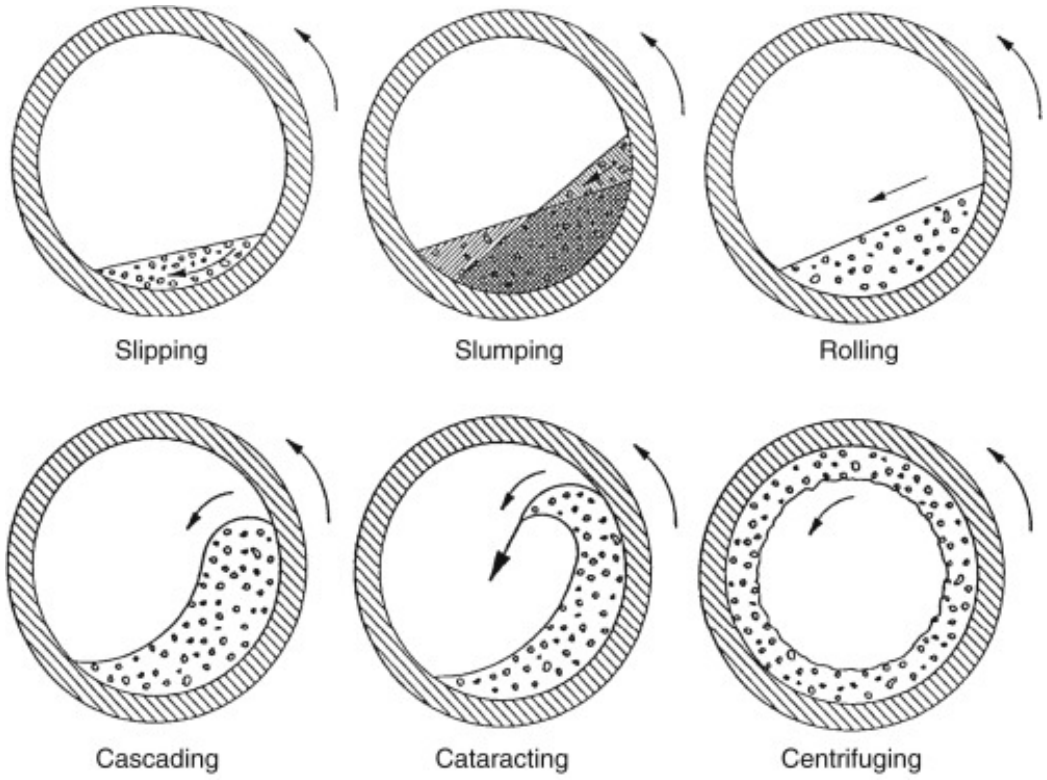

Mode	Fr$(=\omega^2 R/g)$ at $\phi = 35°$
1. Slipping	$Fr < 1.0 \times 10^{-5}$
2. Slumping	$1.0 \times 10^{-5} < Fr < 0.3 \times 10^{-3}$
3. Rolling	$0.5 \times 10^{-3} < Fr < 0.2 \times 10^{-1}$
4. Cascading	$0.4 \times 10^{-1} < Fr < 0.8 \times 10^{-1}$
5. Cataracting	$0.9 \times 10^{1} < Fr < 1$
6. Centrifuging	$Fr > 1.0$

Figure 1.3.2: The different transverse motions of a rotary kiln in cross-sectional plane[3].

1.3.1 Mathematical Modelling Setup

By using computational fluid dynamics (CFD) a flow model can be built that solves transport equations. With this flow model the evaluation of a rotary kilns feature such as mixing degree, temperature profile, bed behaviour and bed behaviour can be performed without the need of building it. From the flow model, an idea of how the operational performance can be seen which helps the design

of the rotary kiln becoming more efficient. This in turn, may reduce the impact of the amount of materials used in the building of the rotary kiln as well as the amount of energy used during operations[5].

1.4 Aim of this thesis

The aim of this master thesis projects is to investigate the parameters affecting the flow regime while also investigating the temperature profile to see its impact of the material properties. This will be achieved by using a continuum modelling framework established by CFD in COMSOL 5.5. As the movement in the axial direction is less significant than the radial direction when investigating the bed behaviour, a two-dimensional suspension model will be created to simulate the flow regimes that is to be described in the next section. A simulation environment will be established to study the flow regimes described in figure 1.3.1 and 1.3.2 and to investigate the temperature profile to see the impact of the material properties. This simulation environment to be created will be used to study the effects of particle size, particle density, rotation speed and degree of filling within the rotary kiln. In this work, the material to be considered general solid material characterised by a particle size and its thermal properties (thermal conductivity, heat capacity, density). The particles are assumed to be spherical and to be of uniform size. The material properties in this work represent typical values found in calcination with rotary kilns.

Chapter 2

Theory

In this section an introduction on how to compute granular flow in CFDis given. In addition, the Philips et. al. (1992) suspension model will be explained in detailed, including the sedimentation flux that has been added later by Acrivos & Zhang.

2.1 Computing granular flow in CFD

During a study of concentrated suspensions of neutrally buoyant spheres in a Newtonian fluid, Acrivos & Galada-Maria (1980) found that at high solid concentration ($\phi_s > 0.4$) the effective viscosity decreased due to prolonged shearing. Once the shearing had reached equilibrium, the effective viscosity became constant. By applying mercury to the bottom of the Couette gap to hinder the solid particles from escaping it was shown that the viscosity decrease was due to the particle migration. It was also found that after a short period of time that the viscosity eventually reached an equilibrium value due to the particles undergoing shear-induced movements. These movements resulted in a particle flux of high shear to low shear and from regions with high particle concentration to low particle concentration. From this, a mechanism to describe the particle migration was developed. However, they did not measure actual particle concentration profile[6].

It is from here, where Philips et. al. (1992) created a constitutive model to describe the shear-induced migration of solid particles in concentrated suspension based on the mechanism proposed by Acrivos & Leighton (1987) for a Couette gap flow with the experimental data from Abbot et al (1991). The constitutive equation created by Philips et. Al. (1992) was for particle concentration and velocity fields of concentrated monomodal suspensions consisting of two parts. These two parts are a Newtonian constitutive equation where the viscosity is

dependent on the local particle volume fraction and a diffusion equation that accounts for the shear-induced particle migration. This model will be discussed more in detailed in the following section[7].

2.2 Philips et. al. Suspension model

The model created by Philips et. al. starts off by considering a suspension of solid particles with a radius, *a*, in a Newtonian solvent with a viscosity, μ. It is assumed that the particles diffuse within the solvent with a diffusivity, *D*, and that the particle Péclet number is large meaning that the convective transport is more significant than the diffusion transport. The model is as earlier mentioned, divided into two parts. These two parts are the stress tensor of a Newtonian fluid with viscosity as a function of concentration and a second part to describe the motion of particles as a diffusion equation in a flow field[7].

2.2.1 The stress tensor

For Péclet numbers > 1, the viscosity mixture model is expressed as

$$\mu = \mu_c(1 - \frac{\phi_s}{\phi_{max}})^{-2.5\phi_{max}} \tag{2.2.1}$$

where ϕ_s (-) is the volume fractions of the solid particles, μ_c (Pa*S) is the viscosity of the solvent, and ϕ_{max} (-) is the maximum volume fraction where the viscosity diverges. The latter has been chosen to be 0.64 for hard spheres. The stress tensor for a Newtonian fluid is expressed as

$$\tau = -\mu(\phi_s)\dot{\gamma} \tag{2.2.2}$$

where $\dot{\gamma}$ = ∇v+∇v^T is the rate-of-strain tensor (1/s) and $\mu(\phi_s)$ is the effective viscosity given by eq 2.2.1[7].

To find the velocity, *v*, and pressure, *p* fields for a given distribution of particles the linear momentum conservation and continuity equations are solved which are expressed as

$$\nabla \cdot \tau + \nabla p = 0 \tag{2.2.3}$$

$$\nabla \cdot v = 0 \tag{2.2.4}$$

with the use of appropriate boundary conditions for the velocity at solid surfaces. These boundary conditions may include no slip or a slip from an appropriate expression at solid surfaces[7].

Looking at the diffusion equation there are potentially many important interactions that could take place for concentrated particles in suspension. The term, "interaction" will now be referred to as the influence of motion one particle has on another particle for the remainder of this section. If it is assumed that the smooth spherical particles will be used, the two main interactions will be a reversible and an irreversible one. In the case of the reversible one, the particle will return to its original streamline once after the interaction itself. However, in order to have a net migration of particles from regions of high to low shear rate, there needs to be an irreversible interaction that results in the particles not to return to their original streamline[7].

It should be noted that the smoothness of the spherical surface plays an important role for the two-body interactions. This is due to the effect of roughness affecting the reversibility which is an important parameter to consider in reality. Also, there are irreversible three-body interactions that may occur as well. However, it has been found that these are an order of magnitude lower than the observed particle migration phenomena. Thus, only the effects from irreversible two-body interactions are considered[7].

2.3 Theory of diffusion equations

2.3.1 Effect of spatially varying interaction frequency

The first irreversible interaction to be formulated is the one describing the spatially varying interaction frequency. This interaction occurs due to collisions between two bodies when they are suspended in adjacent shearing surfaces and move past one another. The particle that experiences a high number of collision from one direction than the other will migrate normal to its shearing surface to a location where less frequent collisions occur. Assuming that the particles in a concentrated suspension undergoing shearing motion move affinely on average, then the number of collisions experiences will scale as $\dot{\gamma}\phi_s$, where $\dot{\gamma}$ is the magnitude of the local shear rate. Assuming that the collision frequency occurs over a distance O(a), the variation is then given as $a\nabla(\dot{\gamma}\phi_s)$. The particle migration velocity is assumed to be linearly proportional to the variation of collision frequency and that each of these two-body interactions results in a displacement of O(a) leading to the final expression for the expression spatially varying interac-

tion frequency flux, N_c

$$N_c = -K_c a^2 \phi_s \nabla(\dot{\gamma}\phi_s) = -K_c a^2(\phi_s \nabla\dot{\gamma} + \dot{\gamma}\nabla\phi_s) \tag{2.3.1}$$

where K_c is an empirically determined coefficient that is determined experimentally and is shear-induced[7].

From eq 2.3.1, it is seen that if there is no concentration gradient, particle migration will still occur if one of the particles moves more rapidly than another particle on one of its side as it will give rise to variation of a high number of particle interactions on the side with the higher $\dot{\gamma}$. Similarly, it is seen that if there is a concentration gradient this will give rise to a spatial variation of frequency of interactions. Also, if the shear flow is imitated in a nonhomogeneous suspension with a constant ϕ_s, the first term in eq 2.3.1 will give rise to a flux which in turn will cause a concentration gradient that induces a second flux proportional to $\nabla\phi_s$. Thus, both terms in eq 2.3.1 will in general oppose one another[7].

The second irreversible interaction is caused by varying collision frequencies due to spatially varying viscosity $\mu(\phi_s)$ which is caused by the existence of concentration gradients for the particles. The gradient in viscosity results in a resistance to the motion to be greater for one of the interacting particles than the other one. In the absence of a viscosity gradient, the difference in resistance will cause one the doublets centre of rotation to move from the midpoint of the line joining the spheres centres towards the direction of higher viscosity. If a viscosity gradient where to exist, the doublets would instead have been displaced in the direction of lower viscosity[7].

2.3.2 Effect of spatially varying viscosity

In a similar manner as with the previous flux, N_c, a quantitative flux expression can be derived. It is assumed the drift velocity is proportional to the change in viscosity over a distance of O(a) relative to the overall magnitude of the viscosity $(a/\mu)\nabla\mu$ and that each interaction results in a displacement of O(a) with an interaction frequency scale defined as $\dot{\gamma}\phi_s$. The resulting migration velocity will then scale as $\dot{\gamma}\phi_s(a^2\mu)\nabla\mu$ which when multiplied with ϕ_s and replacing the gradient of viscosity with eq 2.2.1 to express the gradient of concentration in terms of $\nabla\phi_s$ gives the spatially varying viscosity flux, N_μ as

$$N_\mu = -K_\mu \dot{\gamma}\phi_s^2 \frac{a^2}{\mu}\frac{d\mu}{d\phi_s}\nabla\phi_s \tag{2.3.2}$$

where K_μ is a experimentally determined coefficient that that is determined experimentally and is shear-induced. In eq 2.3.2 it is seen that N_μ is independent of the magnitude of viscosity μ which is consistent with the experimental findings that particle migration rates are independent of the viscosity of the suspending fluid[7].

2.3.3 Sedimentation flux

The Philips et. al. suspension model was created for phases with similar densities. However, if the density variation is significant than the mixture will behave differently. Thus, a new flux was introduced called the sedimentation flux, N_g by Acrivos & Zhang. Imagine a mixture with heavy solid spherical particles radius, *a*, suspended in a liquid with a viscosity, μ_c. Assuming that the particle Reynolds number is small the equations of motion is then to an incompressible Navier-Stokes equation expressed in bulk-averaged effective quantities such as the velocity *u* and

$$\rho = 1 + \epsilon\phi_s, \quad \text{where} \quad \epsilon = \frac{\rho_s - \rho_c}{\rho_c} \tag{2.3.3}$$

where ρ is the mixture density, ρ_s is the density of the pure solid phase and ρ_c is the density of the pure fluid phase, ϕ_s, and ϵ is the reduced density difference being their volume fraction. The effective viscosity in the suspension is given by the eq 2.2.1 with the same maximal viscosity of 0.64 as stated earlier[8].

To find the expression for the sedimentation flux a single solid particle in the suspension is considered equal to the product of the Stokes settling velocity of an isolated particle times a monotonically decreasing function of ϕ_s known as the hindrance function, and the single solid particle is relative to the bulk velocity. The sedimentation flux will account for the reduction in settling velocity due to the irreversible particle interactions formulated earlier in eq 2.3.1 and 2.3.2. Thus, the sedimentation flux is expressed as

$$N_g = u_{stokes} f(\phi_s)\phi_s \tag{2.3.4}$$

where the hindrance function and settling velocity are formulated as

$$f \cong \frac{1 - \phi_s}{\mu} \tag{2.3.5}$$

$$u_{stokes} = \frac{2}{9}\frac{a^2(\rho_s - \rho_c)}{\mu_c} \tag{2.3.6}$$

where $f(\phi_s)$ is the hindrance function and u_{stokes} is the Stokes settling velocity[8].

Chapter 3

Modelling

In this section, the implementation of the suspension model into a laminar mixer will be formulated.

3.1 Implementation of the suspension mixer model

Now that all the fluxes describing the suspension of heavy spherical solid particles in a mixer have been defined, a conservation equation can be defined as

$$N_s = N_c + N_\mu + N_b + N_g \tag{3.1.1}$$

where N_s is the total flux of a particle and N_b is the Brownian diffusion flux. Since it was assumed earlier that the Péclet number is very large, the Brownian diffusive flux can be neglected as the convective forces are more significant than the diffusive forces[7][8].

Eq 3.1.1 is only valid for predicting migration normal to shearing surfaces in unidirectional shear flows where the flow field is characterised by a local shear rate $\dot{\gamma}$. Also, only the particle radius, *a*, appears as the length scale in eq 2.3.1, 2.3.2 and 2.3.4. Thus, it is assumed that $a \ll L$, where *L* is the characteristic length scale of the flow system. Both eq 2.2.2 and eq 3.1.1 will act as the conservation equation for this system[7].

The momentum transport equation for a laminar incompressible flow reads as

$$\begin{aligned}\frac{\partial j}{\partial t} + \rho(j \cdot \nabla)j + (\rho_s - \rho_c)(j_{slip} \cdot \nabla)j = -\nabla p - \nabla \cdot \mu(\nabla j + (\nabla j)^T \\ +\rho g - \nabla \cdot [(\rho_s + \rho_c - \rho)u_{slip} j_{slip}^T] - \rho_c \epsilon (j \cdot \nabla) j_{slip}\end{aligned} \tag{3.1.2}$$

where *j* is the volume-averaged mixture velocity (m/s), *p* is the pressure (Pa),j_{slip} is the slip flux (m/s), *g* is the acceleration of gravity (m/s^2), and u_{slip} is the relative velocity between the two phases (m/s)[9]. The continuity equation for the mixture model is

$$\nabla \cdot j = 0 \tag{3.1.3}$$

The transport equation for the solid phase volume fraction is given as

$$\frac{\partial \phi_s}{\partial t} + \nabla \cdot (\phi_s u_s) = 0 \tag{3.1.4}$$

where u_s is the solid mass phase velocity which is given by $u_s = j + (1 - \phi_s)u_{slip}$. This is where the total flux that was derived earlier will be implemented. The slip velocity between the phases will be described as a particle flux which rewrites the solid phase transport equation to

$$\frac{\partial \phi_s}{\partial t} + \nabla \cdot (\phi_s j + \phi_s(1 - \phi_s))u_{slip} = -\nabla \cdot N_s \tag{3.1.5}$$

When comparing eq 3.1.5 with the previous equation eq 3.1.4 it is seen that this is only true if

$$u_{slip} = \frac{N_s}{\phi_s \rho_s (1 - \phi_s)} \tag{3.1.6}$$

The shear rate tensor, $\dot{\gamma}$, (1/s), is defined as

$$\underline{\dot{\gamma}} = \nabla j + \nabla j^T \tag{3.1.7}$$

and the shear rate tensor magnitude is described as

$$\dot{\gamma} = \sqrt{\frac{1}{2}(\underline{\dot{\gamma}} \cdot \underline{\dot{\gamma}})} \tag{3.1.8}$$

which for a 2-dimensional model is given as

$$\dot{\gamma}_{2D} = \sqrt{\frac{1}{2}(4j_{xx}^2 + 2(j_{xy} + j_{yx})^2 + 4j_{yy}^2)} \tag{3.1.9}$$

3.2 Heat profile model

As the bed of the rotary kiln contains various materials, a heat profile is also something that is to be investigated to investigate the heat transfer effects[10][11][12][13][14].

The generalised heat balance equation for both the solvent and solid phase is defined as

$$\rho_i C_{p,i} \frac{\partial T_i}{\partial t} + \rho_i C_{p,i} u_i \nabla T_i = -\nabla q_i \tag{3.2.1}$$

$$\nabla q_i = k_i \nabla T_i \tag{3.2.2}$$

where subscript, *i*, stands for solid, *(s)*, or solvent, ρ_i stands for the density, *(c)*, $C_{p,i}$ is the specific heat capacity (J/(kg*K)), u_i the velocity for the specific phase given from the momentum equation (m/s), q_i the heat flux (J//m^2*s)), and k_i the thermal conductivity (W/(m*K))[15].

To analyse the sensitivity of the heat conductivity and specific heat capacity, a dimensionless parameter θ is introduced to show how the temperature varies until steady state is reached. It is defined as

$$\theta = \frac{T_{s,min}(t) - T_{s,0}}{T_w - T_{s,0}} \tag{3.2.3}$$

where $T_{s,min}$*(t)* is the minimum temperature of the solid phase at a given time, $T_{s,0}$ the initial temperature of the solid temperature and T_w the maximum temperature given from the wall of the rotary kiln. It is seen that once θ = 1, the solid bed temperature will have reached a homogeneous temperature profile equal to the wall temperature

CFD is a widely used numerical method to solve problems involving fluid dynamics that uses the numerical method finite element method (FEM) to solve governing equations. FEM attempts to solve partial differential equations through approximation which results in a linear equation system with discrete values of primary variables as unknowns that is solved numerically. This is done by letting dividing the structure into so called finite elements (discretisation) which are then coupled to nodes. Afterwards, an approximative solution is gathered for each element which is often based on linear or quadratic functions[16].

The discrete structure is often referred to as mesh and the process to create a mesh is the mesh generation. One can think of FEM containing four steps for computational modelling[16].

- Modelling of the geometry
- Meshing (discretisation)
- Specification of material properties

- Specification of boundary, initial, and loading conditions

Modelling of the geometry is done by using curved surfaces/lines to imagine the geometry and boundary of the structure. This means in the terms of FEM that it is made up of a mesh which is essentially collection of elements, and the curved lines/surfaces may be approximated by piecewise straight lines or flat surfaces. Thus, it is suitable to modify the mesh near surfaces to ensure as close as possible approximation of the geometry. However,it should be notated that this will result in the computational time increasing [16].

Meshing is performed because engineers want to solve a very complex problem that is unpredictable using functions across the whole domain of the problem. Meshing will allow us to approximate the functions into smaller elements so that the problem domain is now divided into smaller elements/cells using a set of grids or nodes. Now the solution can be approximated using simple functions such as polynomials.

Material or medium properties are taken into account as systems may consist of multiple components where each component can be of different materials. There could even exist a single component made of multiple materials such as a composite materials. The properties of materials are therefore defined for a group of elements or for individual elements if needed. Knowing the material properties can allow the system to define regions of the geometry where the data applies. Boundary, initial and loading conditions play an important role in the simulation. By defining them we can solve the system itself, this is kind of self-explanatory[16].

Once a FEM model has been created it is then used in a solver that will solve the discretised system of equations at the nodes of the mesh. The solver has two important considerations that needs to be taken into account when solving a FEM model. The first one being that the storage required and the second one is the central processing unit (CPU) time needed which will determine how long the simulation takes[16]

Chapter 4

The Experimental Method

In this section the experimental method for the flow regime and the heat flow analysis will be given.

4.1 The flow regime analysis

In this study, COMSOL Multiphysics 5.5. was used with the Mixture Model, Laminar Flow physics with a user-defined slip velocity model to simulate the 2-dimensional cross section of a rotary kiln. The parameters to study for the flow regime are as followed

- Viscosity of the solvent
- Experimental coefficients
- Bed behaviour diagram
- Solid particle radius
- Solid particle density

which will each be described in the following sections.

The boundary conditions will change depending on the parameter that will be investigated. In table 4.1.1, the default input data is shown. When one parameter is to be investigated, the other parameters will be set to the default value. All of these values were taken with different processes in mind due to the nature of variety in a rotary kiln. The default bed behaviour that will be used for each parameter unless specified is the rolling mode as seen in figure 1.3.2. Each simulation will run until steady state has been reached for the bed.

Table 4.1.1: The default values to be used for the rotary kiln if nothing else has been stated.

Parameter	Default value	References
Radius of kiln	2.54 [cm]	[17]
Initial volume fraction	0.59 [-]	[17]
Maximum volume fraction	0.64	[18]
Gas density	1.29 [kg/m^3]	[19][20]
Solid density	2000 [kg/m^3]	[21][22][23][19][20]
Solid particle radius	0.5e-3 [m]	[6]

4.1.1 Gas viscosity

The viscosity of the solvent is to be investigated as the model originally was proposed to be used for solid and liquid phase of similar densities[8][7]. Thus, the impact of the viscosity is needed to be investigated as in eq 2.3.4 the magnitude of the viscosity is taken into account which may affect how strong the sedimentation effect will be.

4.1.2 Experimental coefficient

The experimental coefficients K_c and K_μ that are shear induced coefficients that are experimentally determined is commonly defined as 0.41 and 0.62 respectively for a Couette flow for a solid and liquid phase[7]. As this study will use the mixture model for a rotary kiln with a solid and gas phase, these values will be investigated to see their impact on the flow regime of the solid phase. Once the experimental coefficients have been established, they will be used as the default value for the rest of the simulations. This will be performed by varying the experimental coefficients as seen in table 4.1.2 in a rolling mode seen in figure 1.3.2.

Table 4.1.2: The varying values of the experimental coefficients.

K_c	K_μ
0.41	0.62
1	1
2	2
3	3
4	4
5	5
2	3
3	4
4	5

4.1.3 Bed behaviour modes

As mentioned earlier, the rotation speed and filling degree (volumetric filling of material inside of the rotary kiln) will impact the bed behaviour inside of the kiln seen in figure 1.3.1. As in this study a two-dimensional suspension model was created the known bed behaviour shown in figure 1.3.2 will be studied by changing the filling degree and rotation speed to match that of the literature data seen in figure 1.3.1. The varying values of the filling degree and the rotation speed alongside with the expected mode can be seen in table 4.1.3

Table 4.1.3: The range of values for the filling degree and rotation speed.

Filling degree	Rotation speed	Bed behaviour mode
0.1	2 rpm	Slipping
0.1	5 rpm	Slipping
0.23	2 rpm	Slumping
0.23	5 rpm	Slumping
0.1	35 rpm	Rolling
0.23	35 rpm	Rolling
0.3	35 rpm	Rolling
0.3	150 rpm	Cascading
0.3	170 rpm	Cascading
0.23	190 rpm	Cataracting
0.3	185 rpm	Cataracting
0.1	250 rpm	Centrifuging
0.23	200 rpm	Centrifuging
0.3	250 rpm	Centrifuging

4.1.4 Solid particle density

As a rotary kiln are used in material processing operations as mentioned in section 1.1 the material properties may vary within the feedstock at different times during operation. The difference in particle density will impact the sedimentation flux seen in eq 2.3.4 as well as the Navier-Stokes equation for the volume-averaged flow in eq 3.1.2 and 2.3.3. The density will range from 1000 - 3000 kg/m^3.

4.1.5 Solid particle radius

The particle radius is a parameter that is to be investigated as in the rotary kiln, the radius of particles varies in the feed from 0.1-0.9 mm as the particles that are in the bed range from process to process[21][22][23][24][25]. The change in the radius will, as seen in eq 2.3.1-2.3.4. will affect the impact of the flux on the flow regime. In this study, it is assumed that the solid particles are smooth surfaces that are of the same size and they will range from 0.1 - 0.9 mm.

4.2 Thermal property analysis

After the simulation environment had been developed for the flow regime, the thermal properties were to be analysed by implementing the Heat Transfer for Fluids physics coupled with the previous Mixture Model, Laminar flow physics with the user-defined slip velocity model. In this study, the parameters to be analysed are the thermal properties of the solid phase which will be discussed in the following sections.

4.2.1 Solid and gas phase properties

For this model, the momentum equation will be solved by using the default values found in table 4.1.1 for the same geometry. For the heat transfer, a sensitivity analysis is performed with respect to the thermal conductivity and specific heat capacity of the solid phase. The values used for the two different cases are shown in table 4.2.1. As for the gas phase, the values are chosen for a pure oxygen flow and it can be seen in table 4.2.2. When the thermal conductivity is varied, the specific heat capacity is set to 0.54 (kj/(kg*K)), and when the specific heat capacity is varied the thermal conductivity is set to 0.25 (W/(m*K)).

Table 4.2.1: The specific heat capacity range and thermal conductivity value range for the solid phase.

Parameter	Value range
k_s	1-50 (W/(m*K))
$C_{p,s}$	0.3-.8 (kJ/(kg*K))

Table 4.2.2: The specific heat capacity range and thermal conductivity for the gas phase.

Parameter	Value	References
k_g	50 [mW/(m*K)]	[26]
$C_{p,g}$	1.11 [kJ/(kg*K)]	[27]

4.2.2 Boundary conditions

The boundary conditions for the thermal property analysis are given in table 4.2.3 with the default values in table 4.1.1 for the flow regime.

Table 4.2.3: The boundary conditions to be used for the thermal property analysis.

Variable Name	Parameter Name	Value
Initial Gas Temperature	$T_{g,0}$	200 [C°]
Initial Solid Material Temperature	$T_{s,0}$	20 [C°]
Temperature of the Wall	T_w	650 [C°]

4.3 Model setup

4.3.1 Geometry and mesh of the rotary kiln

In this study, a rotary kiln with a radius of 2.54 cm with smooth spherical particles with a uniform size were used for a 2-dimensional model. The mesh created for the rotary kiln consisting of 6500 elements is shown in figure 4.3.1.

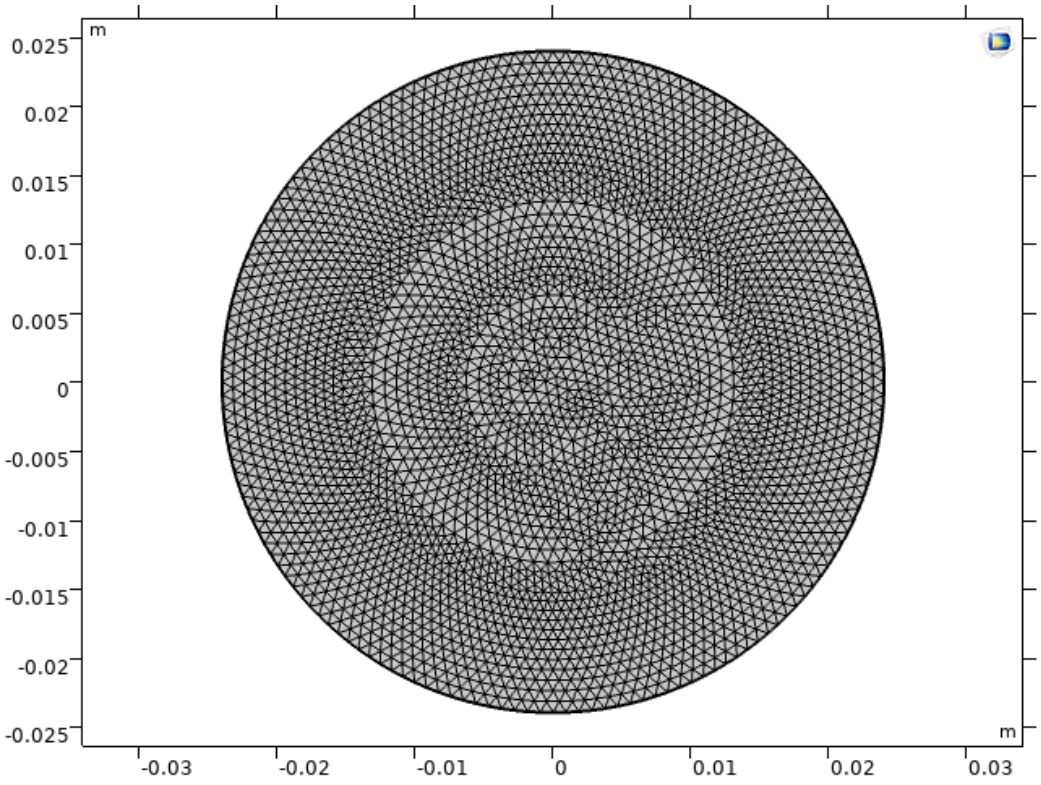

Figure 4.3.1: The mesh of the rotary kiln.

4.3.2 Initial state of particle distribution

The setup of the 2-dimensional model is initiialized with a bed at a certain fill level on 0.59 solid volume fraction. The initial state for a filling degree of 0.23 is shown in figure 4.3.2 where the walls are rotating clockwise to initiate particle motion. It should be noted, that this initial state will vary depending on the filling degree as seen in figure 4.3.3 and figure 4.3.4.

The simulations will be performed by having the outer walls rotating clockwise at a steady rate of 35 rpm unless specified. As the the rotary kiln is centred at (0,0), this corresponds to a velocity of

$$(j_x, j_y) = \frac{110\pi}{60}(y, -x) \tag{4.3.1}$$

The particle flux is zero through the boundaries and there is no slip conditions at all walls.

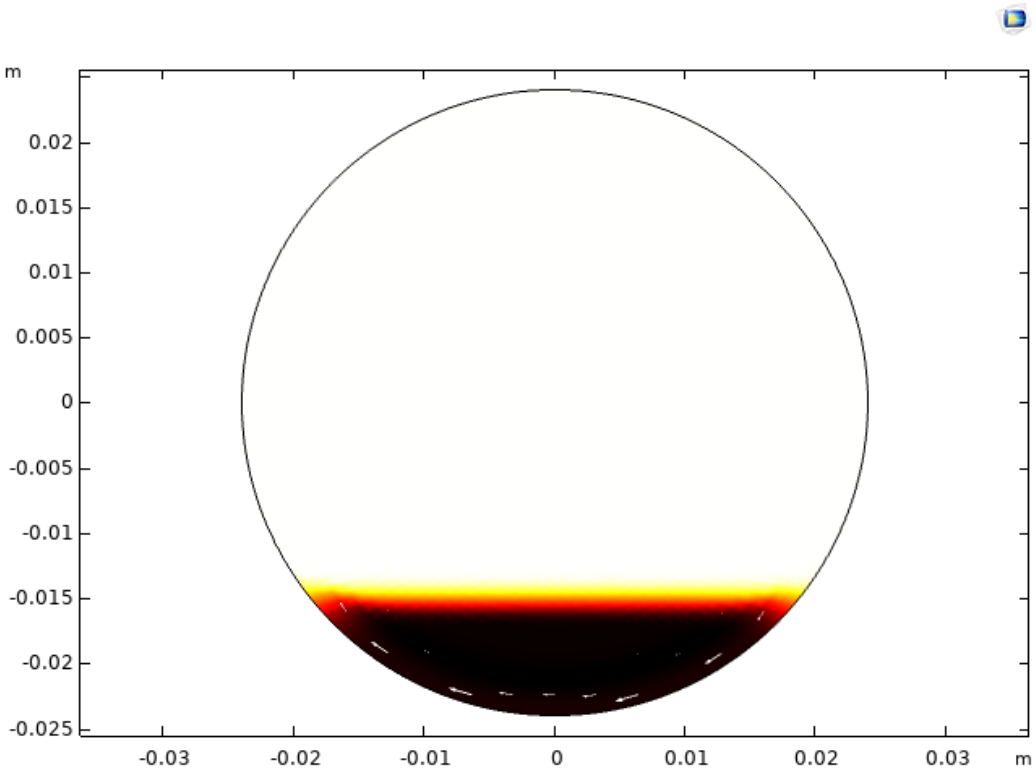

Figure 4.3.2: The initial state of the particles for the rolling mode at 0.23 filling degree.

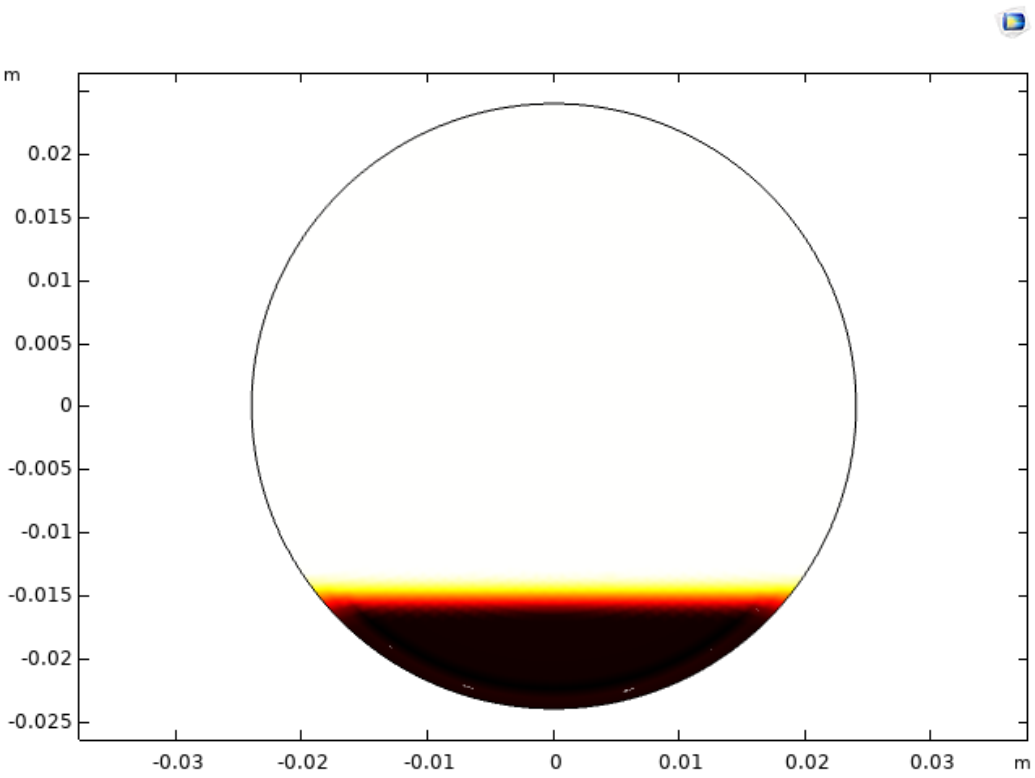

Figure 4.3.3: The initial state of the particles for a filling degree of 0.1.

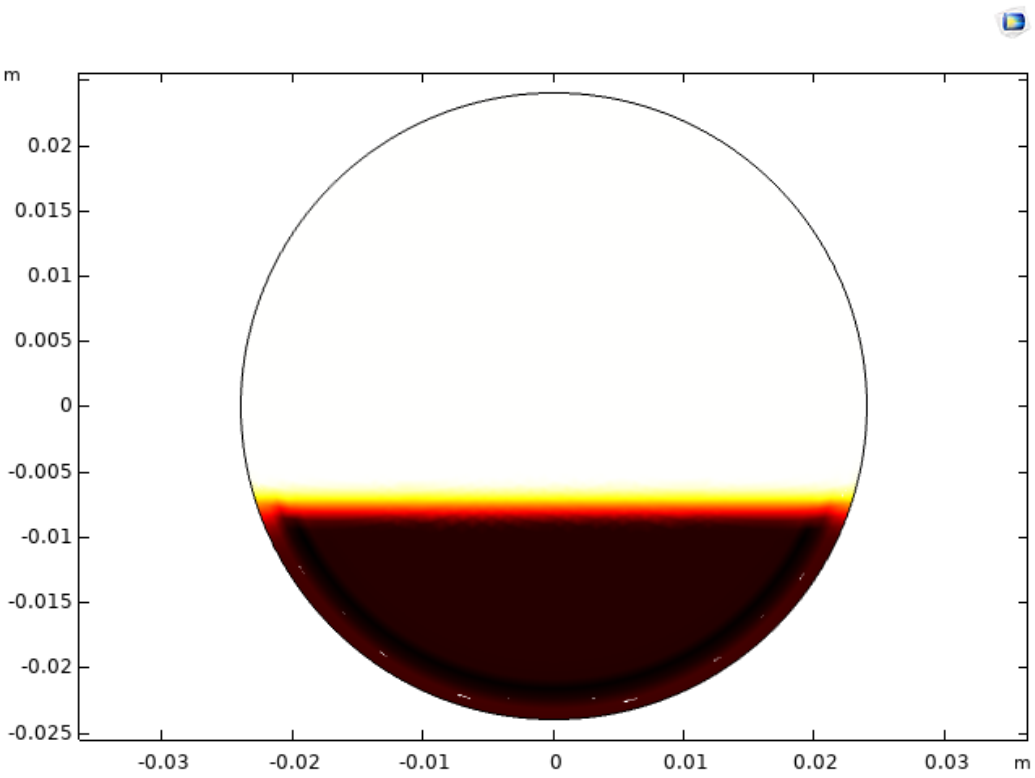

Figure 4.3.4: The initial state of the particles for a filling degree of 0.3.

Chapter 5

Results and Discussion

In this section, the results of both the flow regime and the heat profile will be presented and discussed.

5.1 The limitation of the Philips et. al. model

The original model, was developed for a solid and liquid phase flow in a mixer. Thus, this study aimed at reducing the viscosity of the fluid phase in order to reach that of a gas. It was seen however, that the viscosity could not reach that of a gas. As the viscosity reaches a value of 2.055e-3 [Pa*s], the mixture viscosity starts to increase exponentially until it reaches a plateau which is magnitudes higher than the original value as seen in figure 5.1.1. The reason for this is due to the sedimentation flux equation 2.3.4 and the equation for the mixture viscosity 2.2.1. As the viscosity of the fluid phase is decreased to match that of a gas, the sedimentation flux is increased in as well resulting in the sedimentation flux becoming too large resulting in it pulling the particles in the bed down and hindering movement. This in turn results in the model trying to increase the viscous forces in order to try to find a value in order for the particles to move, but this only results in the system not being able to converge as now the other fluxes will have to become too large to combat the increase of viscosity. Moving on forwards, the viscosity of the gas will be set to 2.055e-2 (Pa*s) as it is the lowest value that was achieved with good convergence.

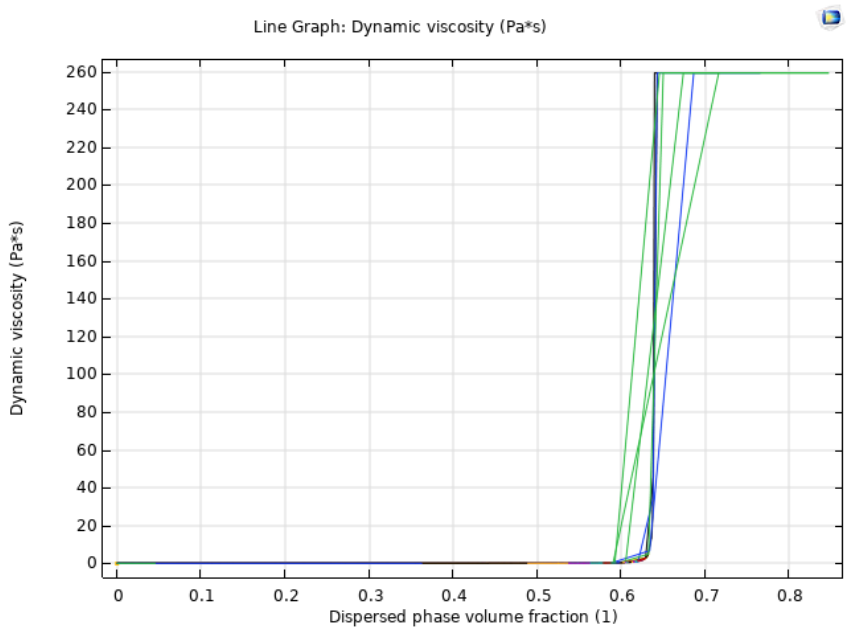

Figure 5.1.1: The mixture viscosity limitation plotted against the concentration of the solid phase.

5.2 Experimental parameters

The first simulation run was of the original parameters in a rolling mode without the rotating inner cylinder. In figure 5.2.1, it can be seen once steady state has been reached that the solid bed will rotate in the same direction as the wall moves. The solid particles in the passive region will rotate to the top of the left wall until they reach a certain elevation and drop down to form the active layer in which the particles will slide down to the bottom until they reach the passive layer again. In other words, the solid bed will renew itself throughout the process by itself. This is typical behaviour of a rolling mode, except for the solid particles travelling from the passive layer that high along the left wall until it reaches the active layer.

The next simulations was performed for investigating how the flow regime would look if the experimental coefficient change. The experimental coefficients, K_c and K_μ, that are shear-induced were investigated for different values that were either the same or different, The results for the same values used can be seen in 5.2.2, 5.2.3 and 5.2.4, and for using different values the results is shown in figures 5.2.5 and 5.2.6 respectively. As the constants are increased, the bed starts to shift more and more towards the centre of the kiln, while still rotating the particle

cluster along the wall to a certain elevation. This can be explained through eq 2.3.1 and 2.3.2 where increasing the experimental parameters will increase their effect on the irreversible collisions. From these simulations, the experimental coefficients were set to K_c = 3 and K_μ = 4 due to the good convergence they produced within the software and having the most similar bed behaviour to the rolling mode. Results regarding the variation of experimental coefficient can be found in Appendix A

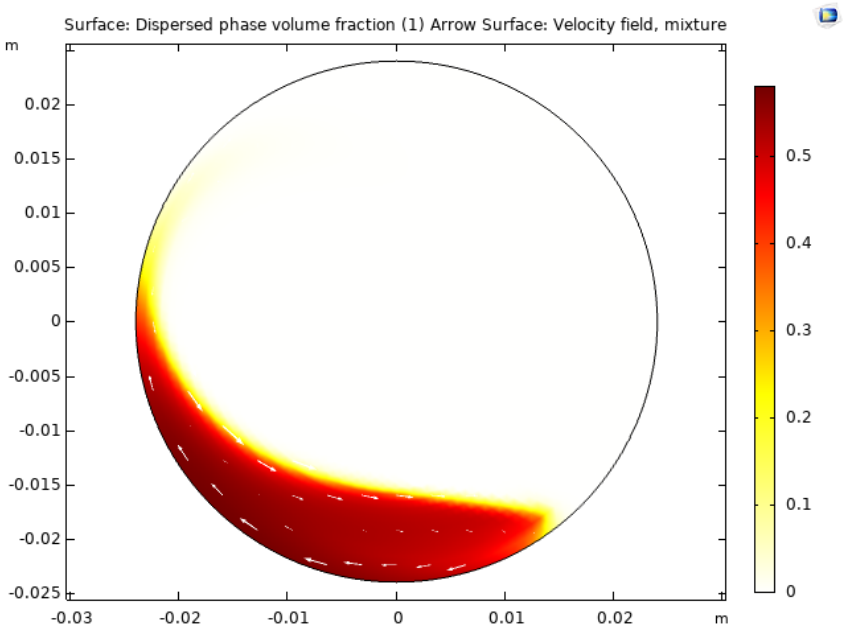

Figure 5.2.1: The flow regime of the bed in rolling mode with K_c = 0.41 and K_μ = 0.62 with the white arrows showing the direction of the rotation.

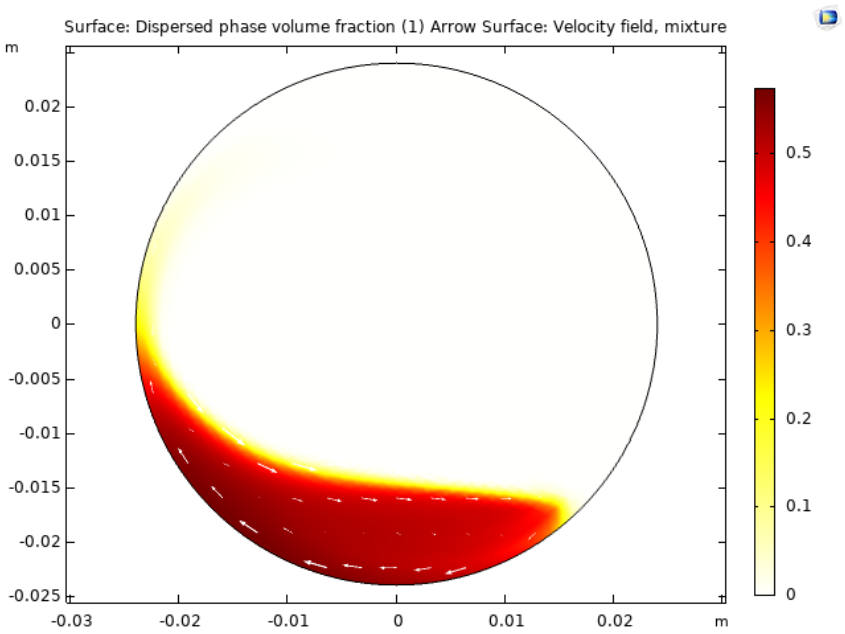

Figure 5.2.2: The flow regime of the bed in rolling mode with $K_c = K_\mu = 1$ with the white arrows showing the direction of the rotation.

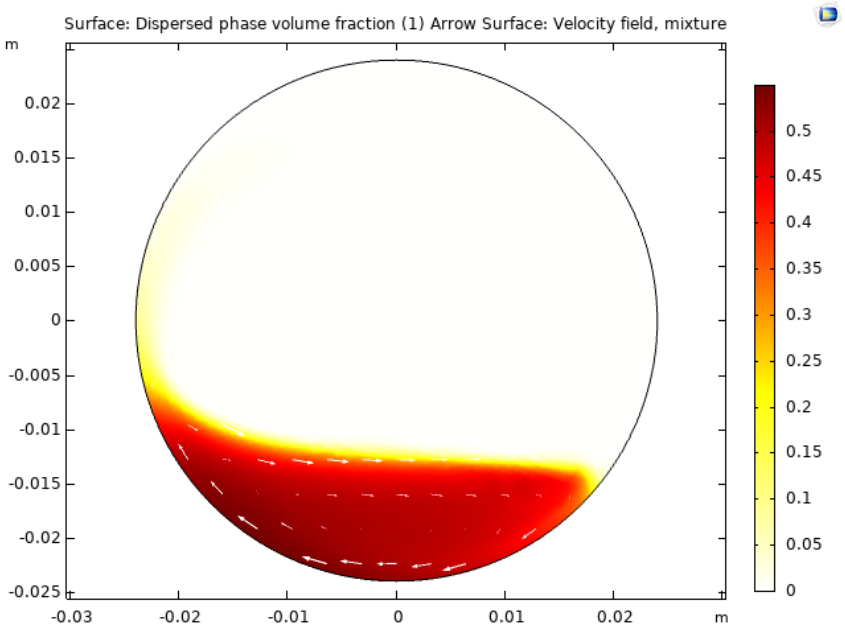

Figure 5.2.3: The flow regime of the bed in rolling mode with $K_c = K_\mu = 3$ with the white arrows showing the direction of the rotation.

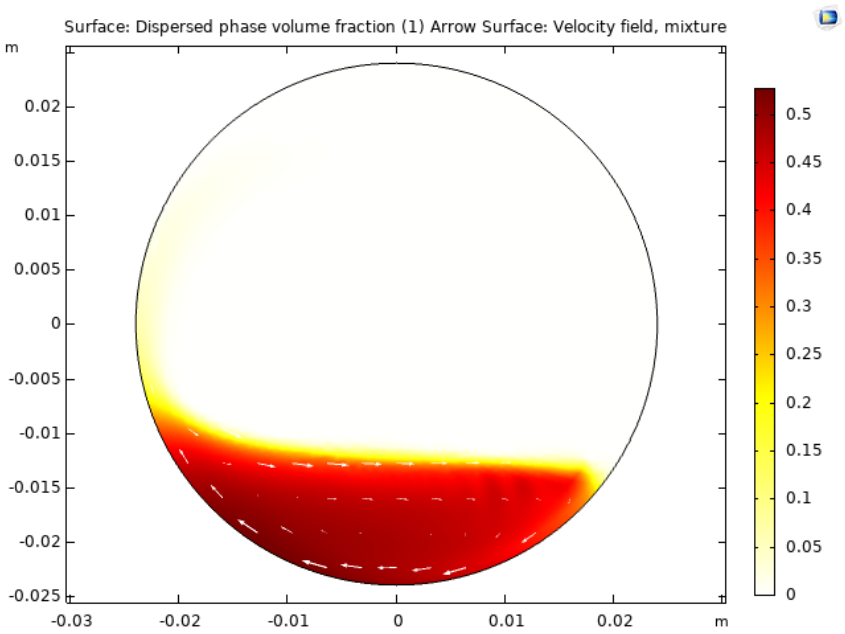

Figure 5.2.4: The flow regime of the bed in rolling mode with K_c = K_μ = 5 with the white arrows showing the direction of the rotation.

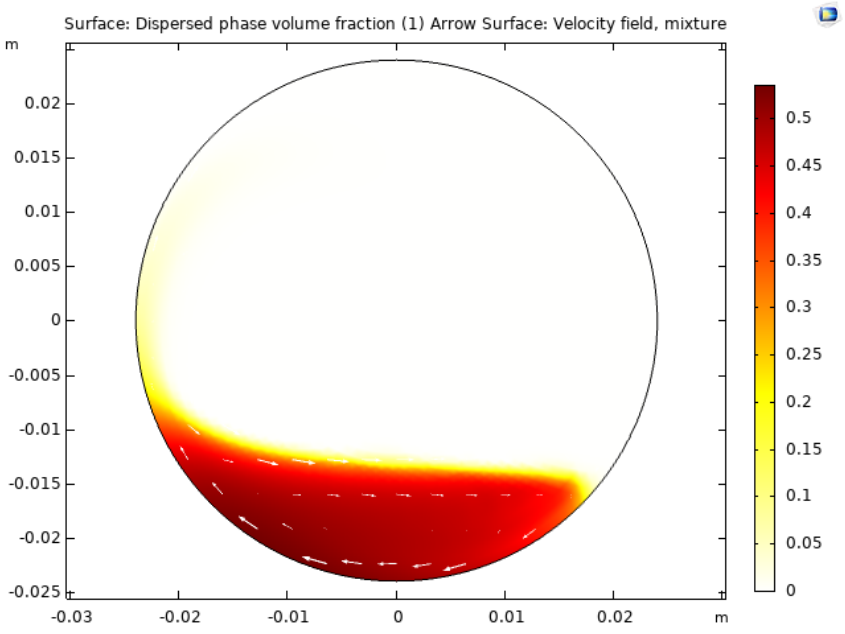

Figure 5.2.5: The flow regime of the bed in rolling mode with K_c = 3 and K_μ = 4 with the white arrows showing the direction of the rotation.

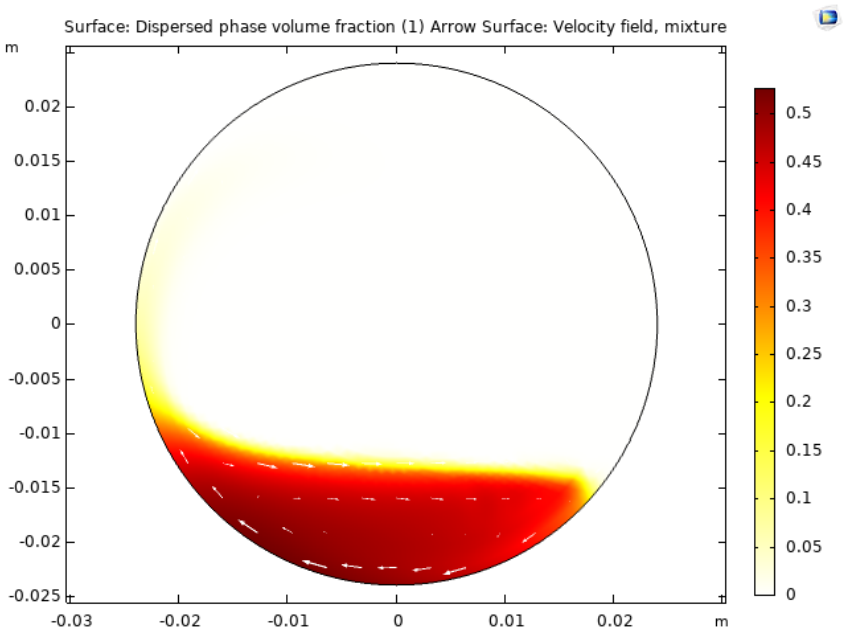

Figure 5.2.6: The flow regime of the bed in rolling mode with K_c = 4 and K_μ = 5 with the white arrows showing the direction of the rotation.

5.3 Solid particle radius

The impact of the solid particle radius can be seen in the figures 5.3.1-5.3.6. It is shown that increasing the particle radius results in the solid phase going from a homogeneous mixture to a rolling mode bed behaviour. This can be explained as the viscous forces becoming larger which is seen in the equations 2.3.1-2.3.2 where increasing the particle radius will increase the effective particle flux. This change in particle radius also affects the sedimentation flux. However, since the sedimentation flux only occurs in the y-axis and the other two fluxes occur in both x-axis and y-axis its effect is smaller until a particle radius of 0.4 mm is reached as seen in figure 5.3.4. From here on, as the particle radius is increased the solid bed phase will not be elevated as high in order to drop down to the active layer. For further proof for the variation between 5e-3 mm to 9e-3 mm see Appendix B.

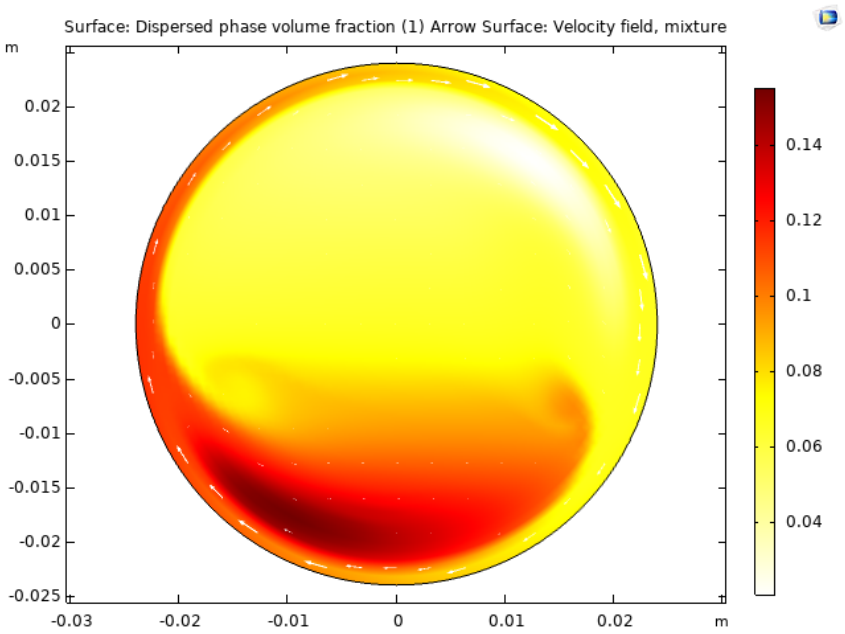

Figure 5.3.1: The flow regime of the bed in rolling mode with a solid particle radius of 0.1 mm with the white arrows showing the direction of the rotation.

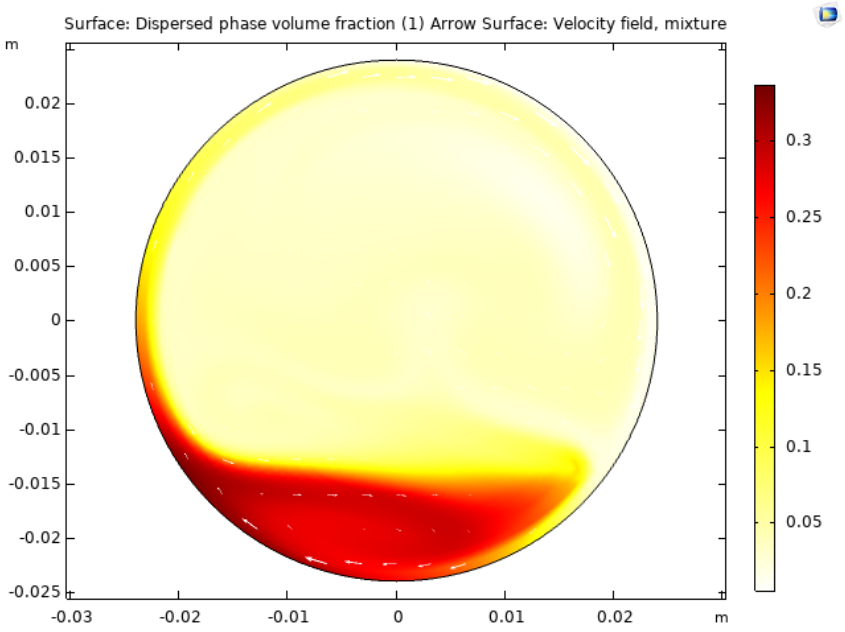

Figure 5.3.2: The solid phase flow regime of the bed in rolling mode with a solid particle radius of 0.2 mm with the white arrows showing the direction of the rotation.

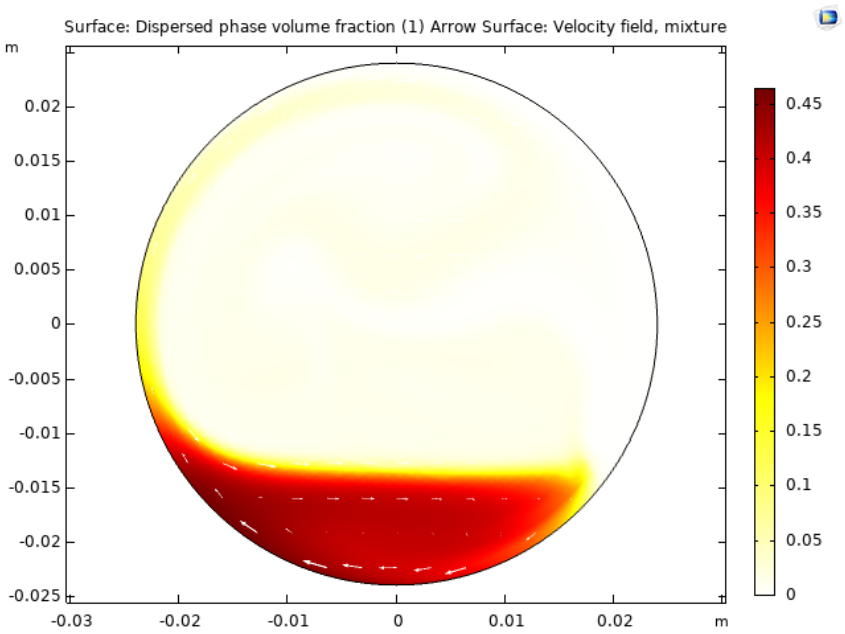

Figure 5.3.3: The flow regime of the bed in rolling mode with a solid particle radius of 0.3 mm with the white arrows showing the direction of the rotation.

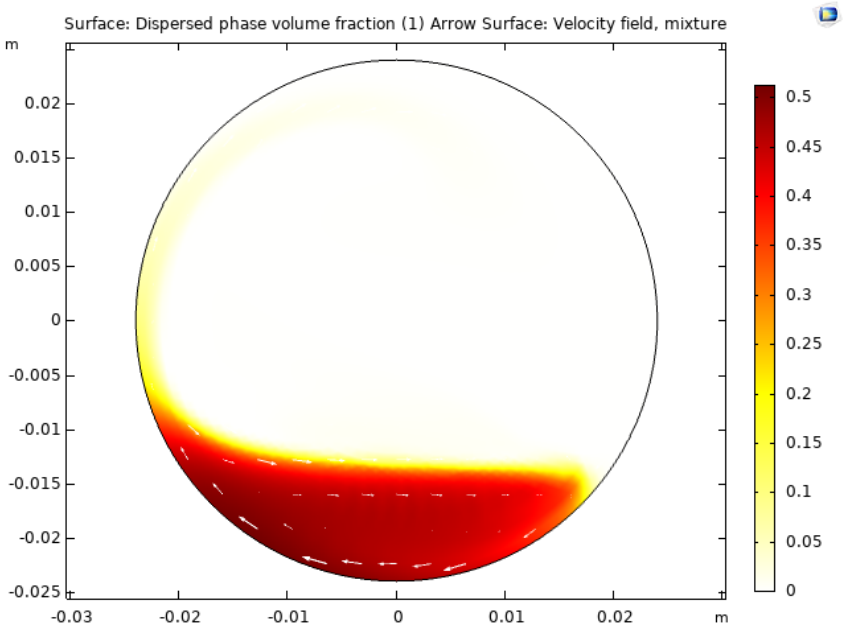

Figure 5.3.4: The flow regime of the bed in rolling mode with a solid particle radius of 0.4 mm with the white arrows showing the direction of the rotation.

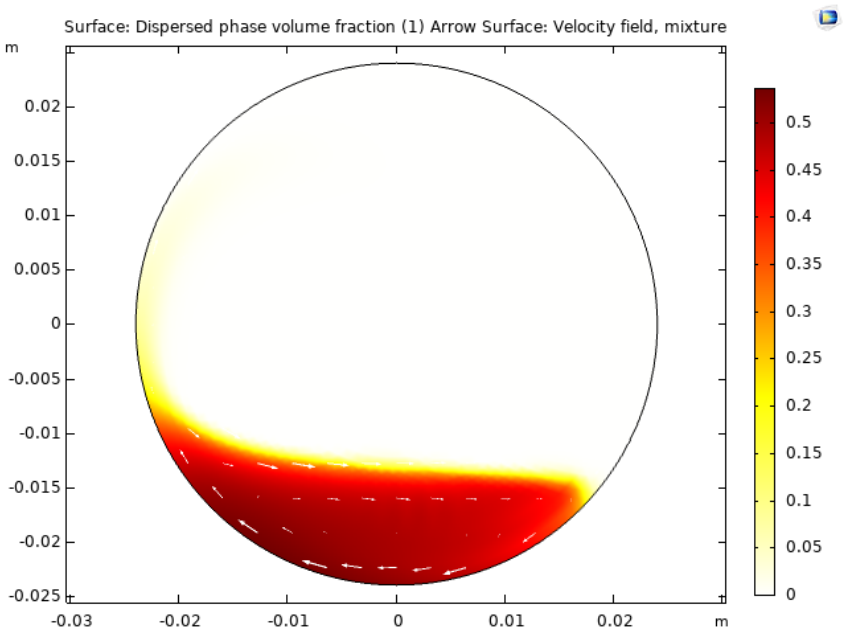

Figure 5.3.5: The flow regime of the bed in rolling mode with a solid particle radius of 0.5 mm with the white arrows showing the direction of the rotation.

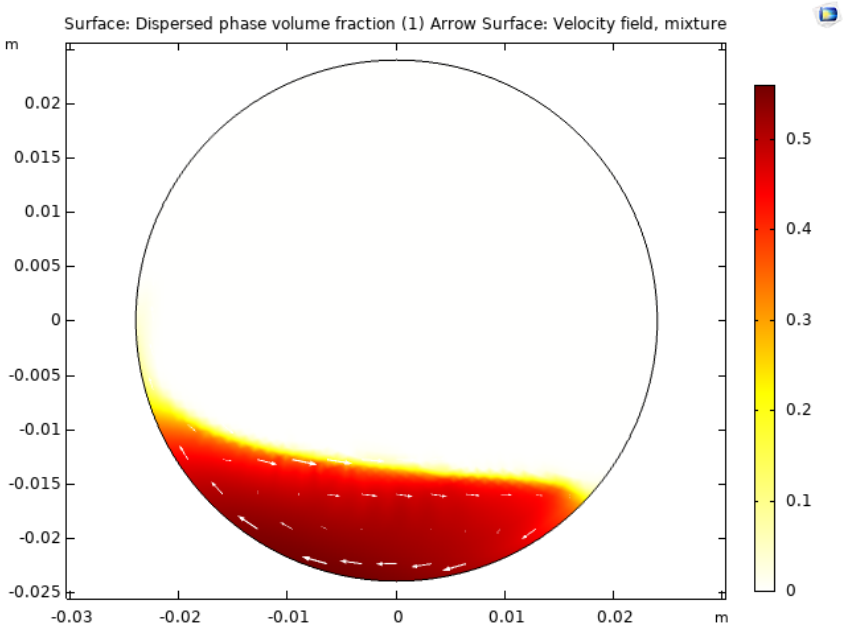

Figure 5.3.6: The flow regime of the bed in rolling mode with a solid particle radius of 0.9 mm with the white arrows showing the direction of the rotation.

5.4 Particle density

As the particle density is increased from 1000 to 3000 kg/m^3, the elevation height that the particles will reach decreases until a particle density of2000 kg/m^3, beyond which an increase in the particle density results in minimal differences to the flow regime. This due to the sedimentation flux seen in eq 2.3.4 that is increasing when the solid particle density is increased. The variation also affects the effective density seen in eq 2.3.3 which in turn will also affect the Navierstokes equation seen in eq 3.1.2 where it will affect *j*. All of the different effects from the increase of particle density is seen in figures 5.4.1-5.4.7 and in appendix C that shows the variation between 2500 - 2750 kg/m^3. The flow regime of the bed will as the particle density is increased, resemble more of a rolling mode due to the sedimentation flux pulling down the particles resulting in a the elevation of particles reducing.

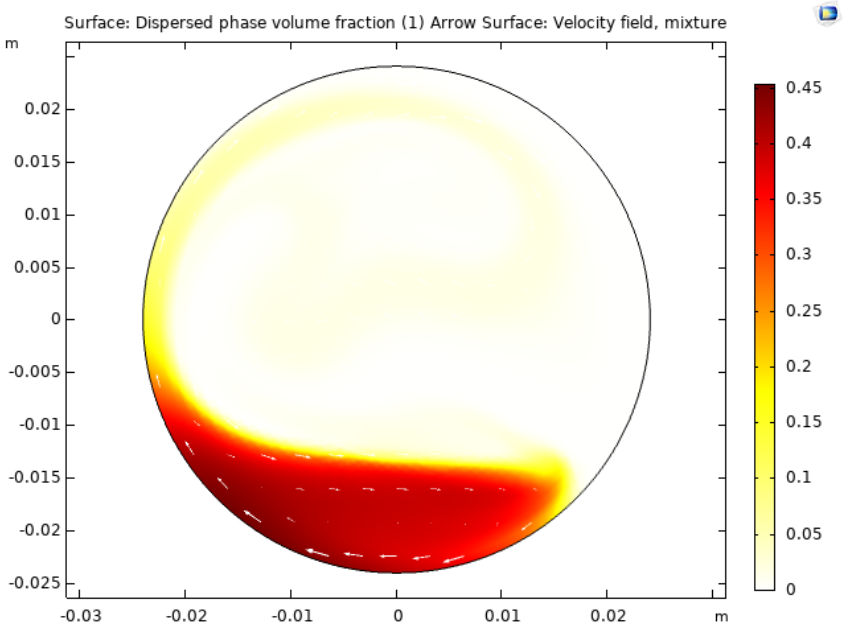

Figure 5.4.1: The flow regime of the bed in rolling mode with a particle density of 1000 kg/m^3 with the white arrows showing the direction of rotation.

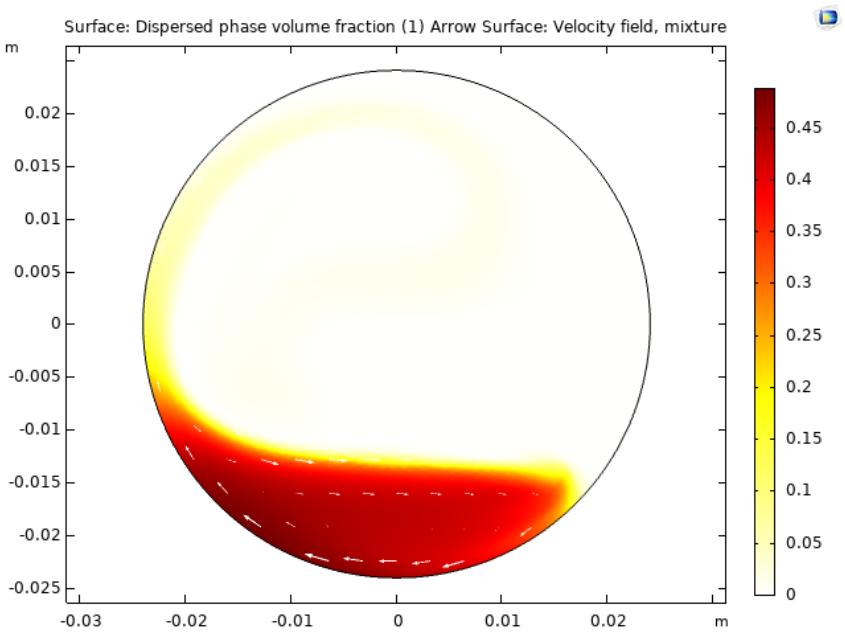

Figure 5.4.2: The flow regime of the bed in rolling mode with a particle density of 1250 kg/m^3 with the white arrows showing the direction of rotation.

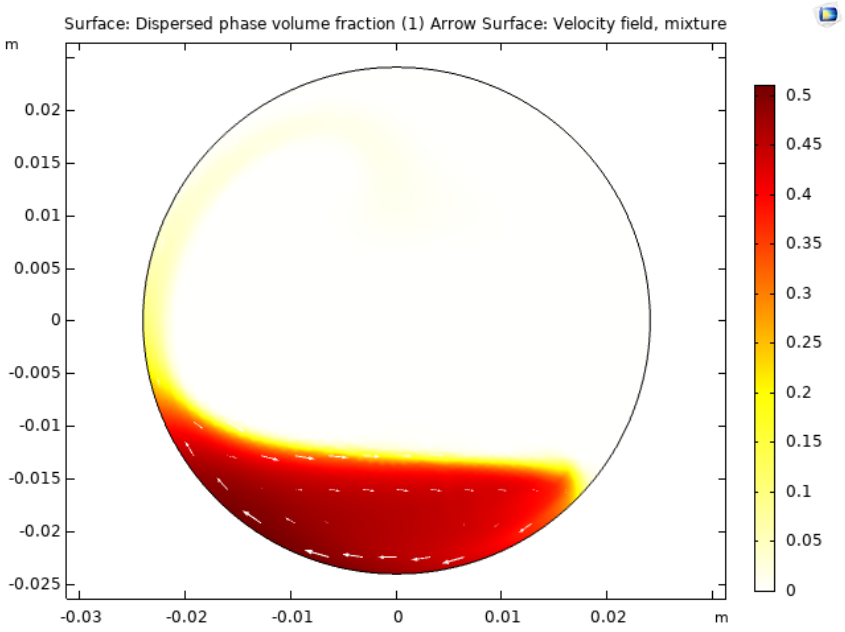

Figure 5.4.3: The flow regime of the bed in rolling mode with a particle density of 1500 kg/m^3 with the white arrows showing the direction of rotation.

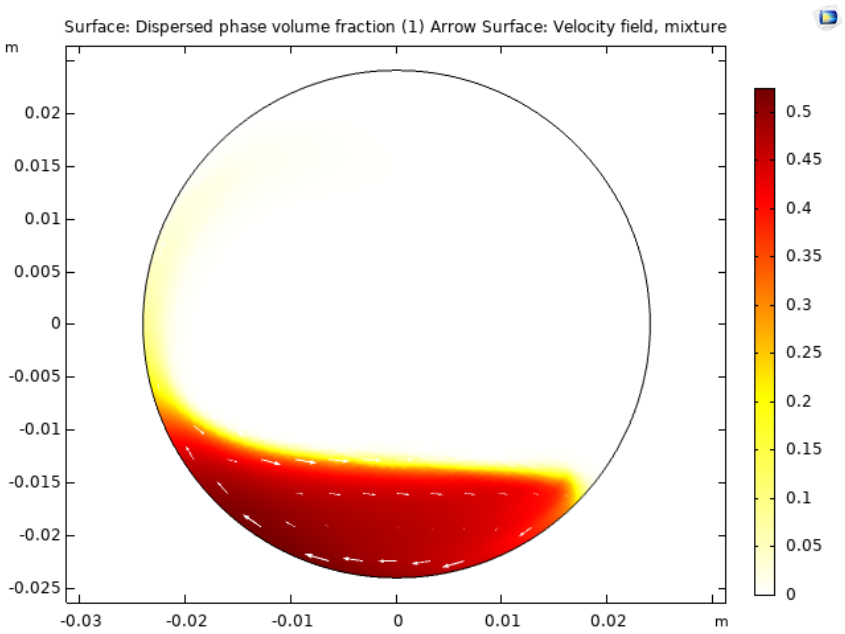

Figure 5.4.4: The solid phase flow regime in rolling mode with a particle density of 1750 kg/m^3 with the white arrows showing the direction of rotation.

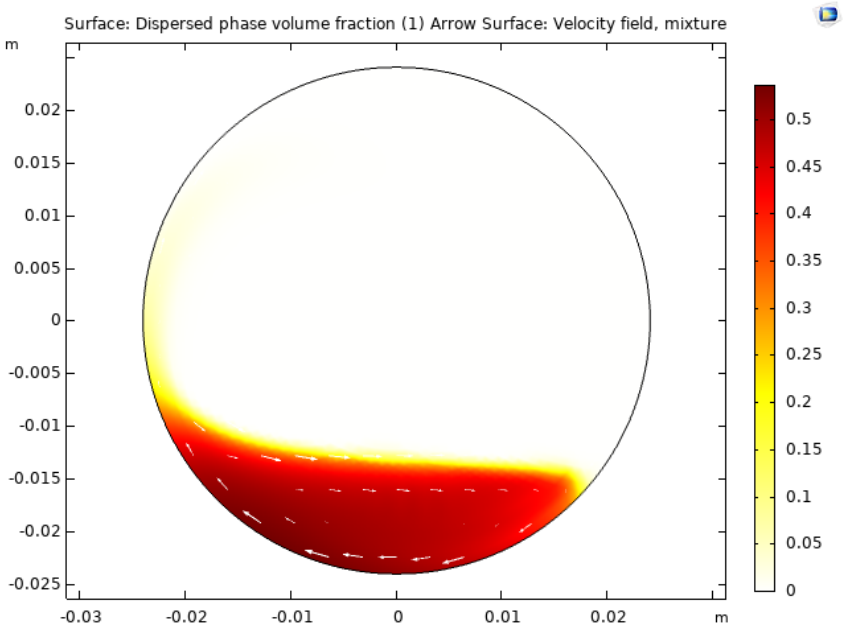

Figure 5.4.5: The flow regime in rolling mode with a particle density of 2000 kg/m^3 with the white arrows showing the direction of rotation.

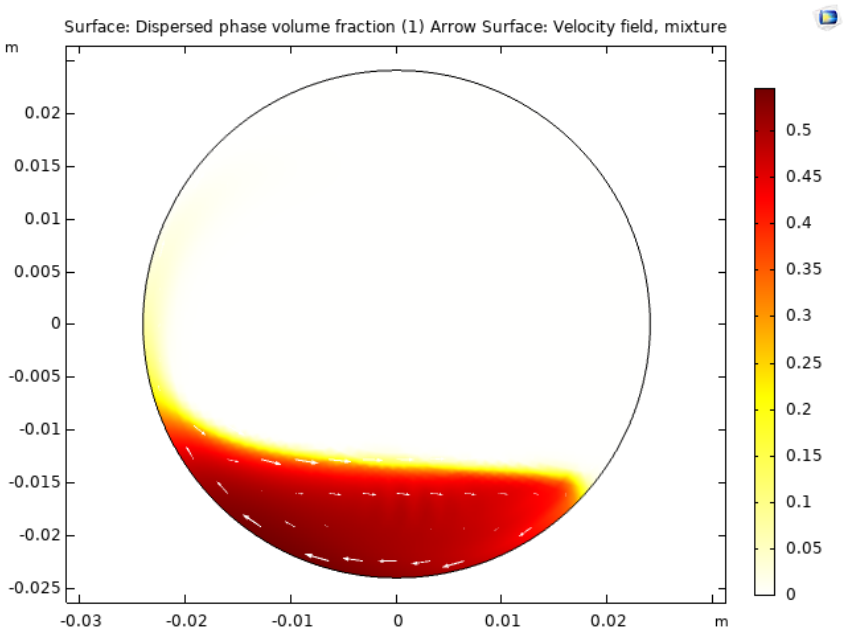

Figure 5.4.6: The solid phase flow regime in rolling mode with a particle density of 2250 kg/m^3 with the white arrows showing the direction of rotation.

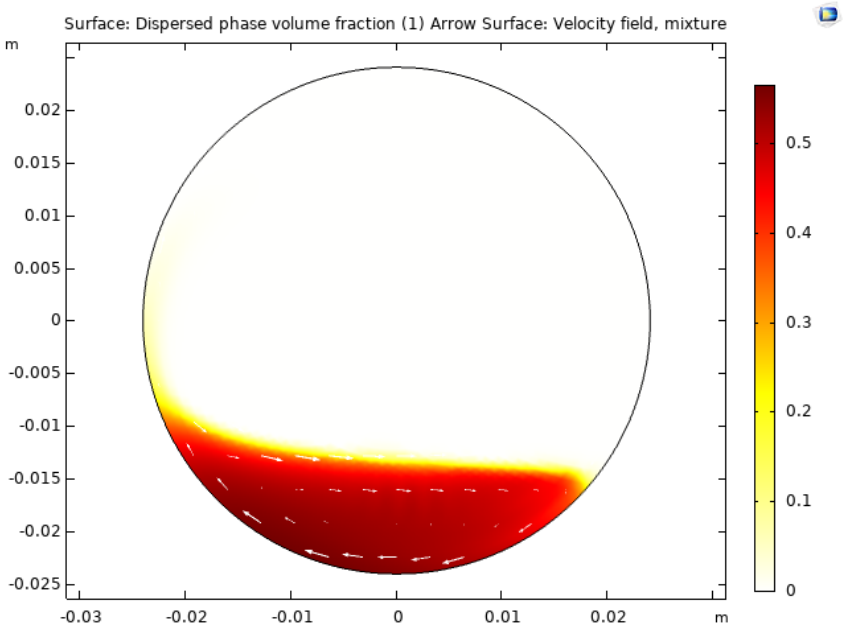

Figure 5.4.7: The flow regime in rolling mode with a particle density of 3000 kg/m^3 with the white arrows showing the direction of rotation.

5.5 Bed behaviour modes

5.5.1 Slipping mode

For the slipping mode, two different rotation speeds were investigated as seen in figures 5.5.1-5.5.2. The passive layer moves along the rotary kiln wall and the active layer is very small compared to the passive layer. The movement is minimal which is what it has been observed in the slipping mode. Thus, the suspension model implemented is able to produce the slipping mode as seen in figure 1.3.2.

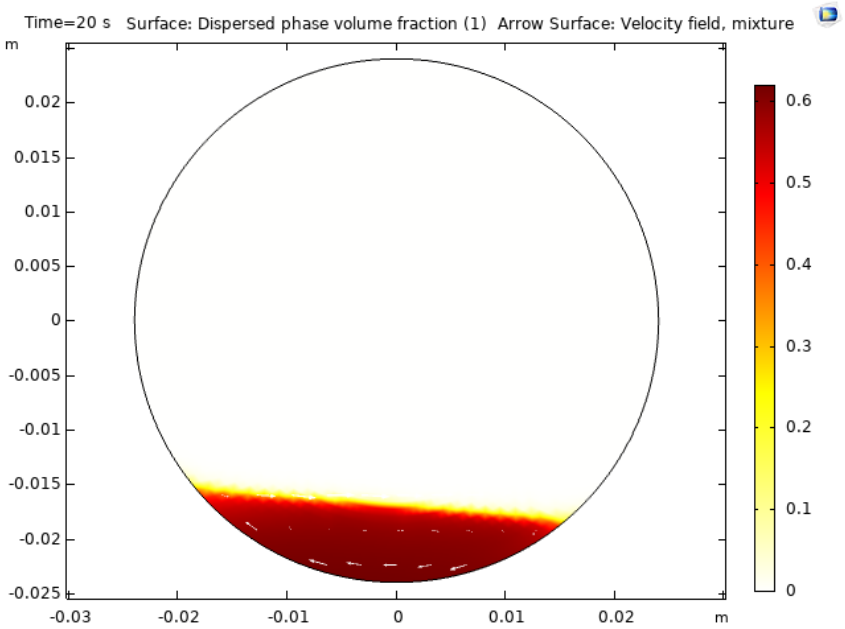

Figure 5.5.1: The flow regime of the bed in slipping mode with a filling degree of 0.1 with 2 RPM the white arrows showing the direction of the rotation.

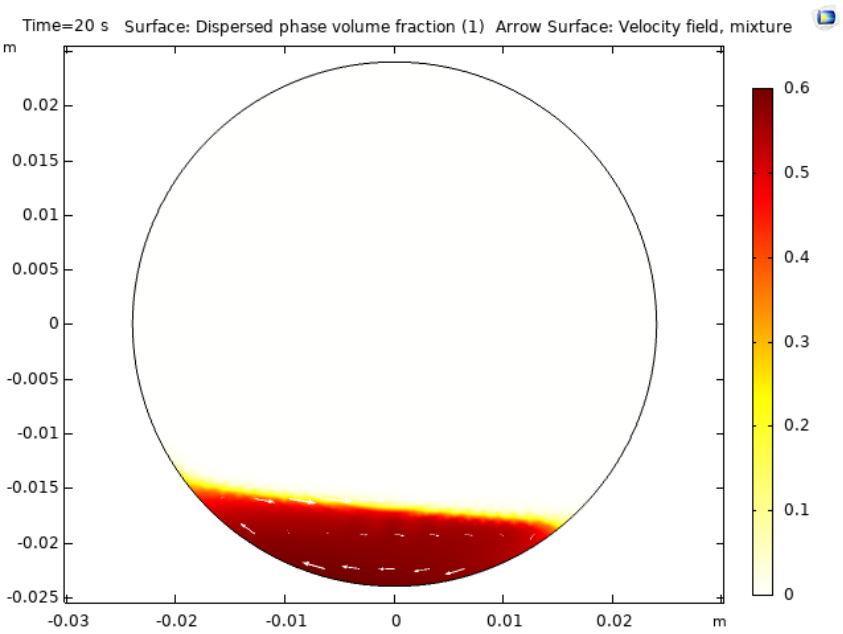

Figure 5.5.2: The flow regime of the bed in slipping mode with a filling degree of 0.1 with 5 RPM the white arrows showing the direction of the rotation.

5.5.2 Slumping mode

The slumping mode of the rotary kiln can be seen in figure 5.5.3-5.5.4. The passive layer of the bed is rotating along the wall of the rotary kiln and the active layer is now larger due to the rotation not being large enough to rotate the passive layer properly. However, a real slumping mode is when the particle bed is moving towards the wall but is elevated and then the particles collapse towards its initial position as seen in figure 1.3.2. Thus, it is seen that even though the rotation speed has increased resulting in a larger passive layer it does not lead to slumping mode.

A reason for why this occurs can be explained through the viscous forces as the only viscosity that is implemented in the model is the viscosity of the fluid as seen in eq 2.2.1. The angle of repose of the bed should increase as the material is elevated until a certain elevation is reached and the material is sheared off and comes to rest at the bottom of the kiln. As this does not happen, it would suggest that the angle of repose of the bed is low due to the viscous forces not being strong enough to keep the materials together. Thus, the bed will simply rotate creatinFg a passive and active layer similarly to a rolling mode.

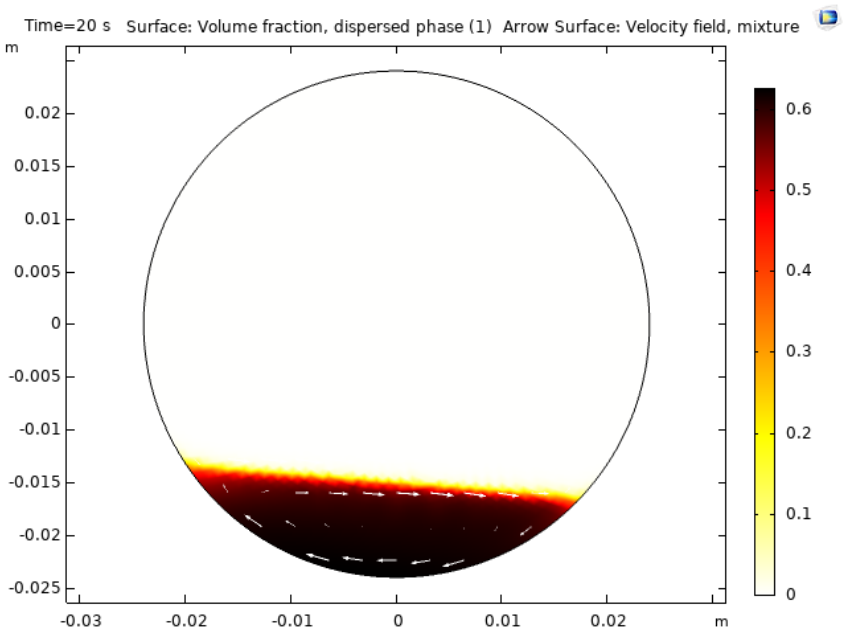

Figure 5.5.3: The flow regime of the bed in slumping mode with a filling degree of 0.23 rotating at 2 RPM and the white arrows showing the direction of the rotation.

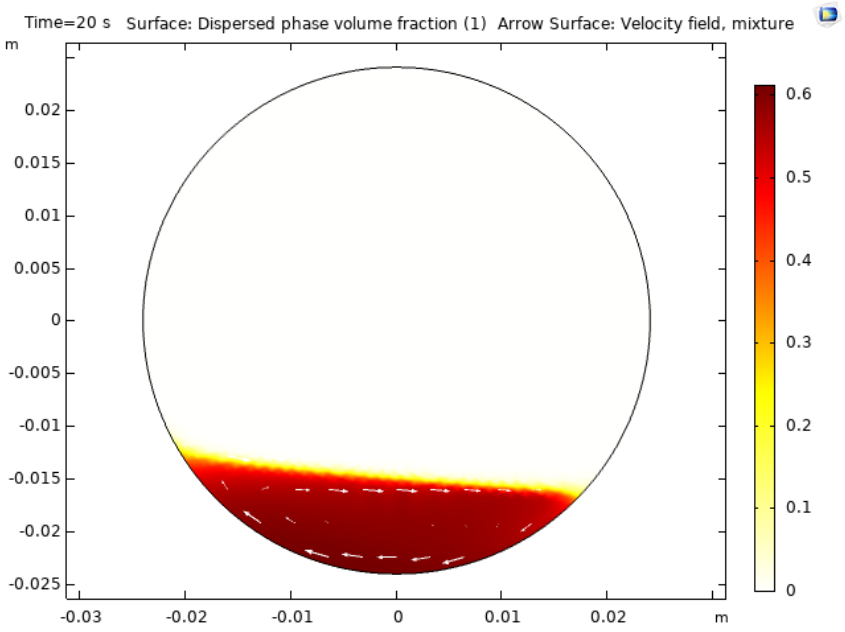

Figure 5.5.4: The flow regime of the bed in slumping mode with a filling degree of 0.23 rotating at 5 RPM and the white arrows showing the direction of the rotation.

5.5.3 Rolling mode

When the rotary kiln is now run in the rolling mode, it is seen that the active layer and passive layer are now greater. The particles will now follow the left wall until a certain elevation is reached to then fall down into the active layer and then roll down into the passive layer again. The bed surface is continuously renewed here. However, the results shown here resemble more of a cataracting mode as the elevation that the particles reach is higher and the particles are now free falling after reaching a certain elevation. Thus, the suspension model is not able to simulate a rolling mode bed behaviour as shown in figures 5.5.5-5.5.14 compared to the figure 1.3.2. For even more results showing that the bed behaviour was similar regardless of filling degree can be seen in appendix D.

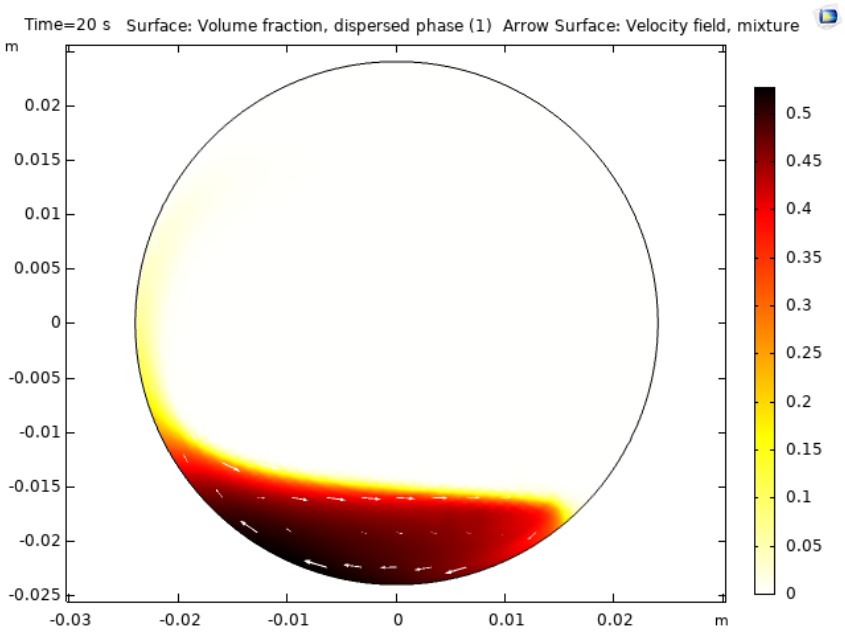

Figure 5.5.5: The flow regime of the bed in rolling mode with a filling degree of 0.1 with 30 RPM the white arrows showing the direction of the rotation.

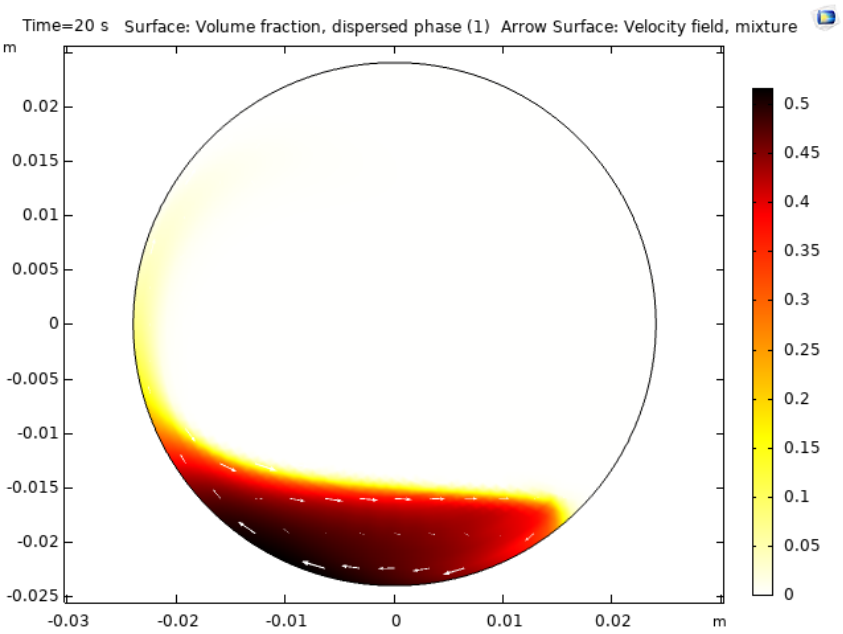

Figure 5.5.6: The flow regime of the bed in rolling mode with a filling degree of 0.1 with 35 RPM the white arrows showing the direction of the rotation.

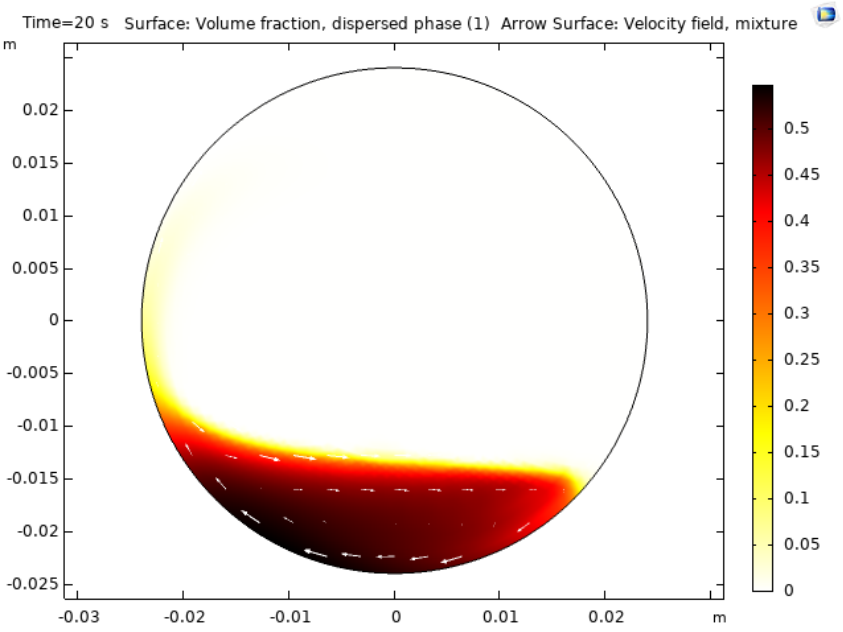

Figure 5.5.7: The flow regime of the bed in rolling mode with a filling degree of 0.23 with 30 RPM the white arrows showing the direction of the rotation.

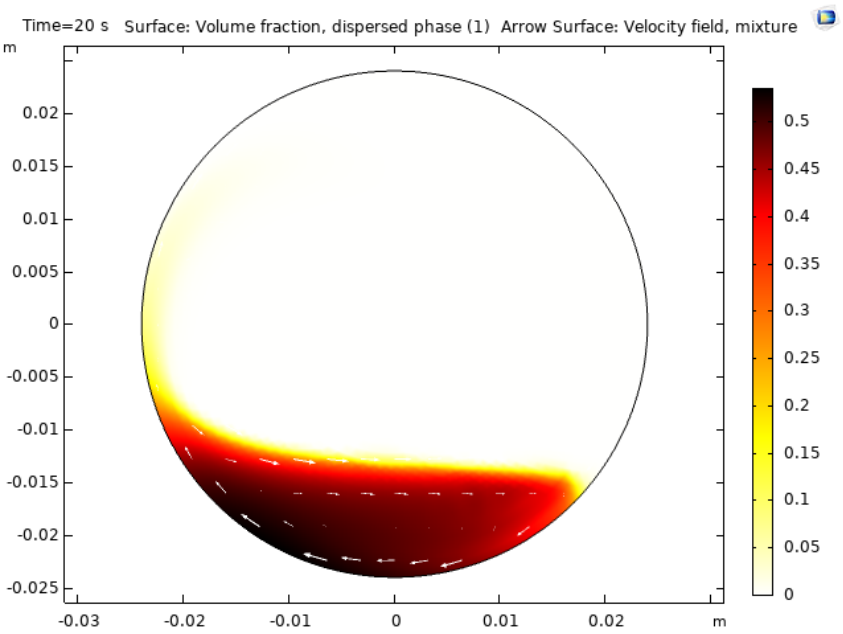

Figure 5.5.8: The flow regime of the bed in rolling mode with a filling degree of 0.23 with 35 RPM the white arrows showing the direction of the rotation.

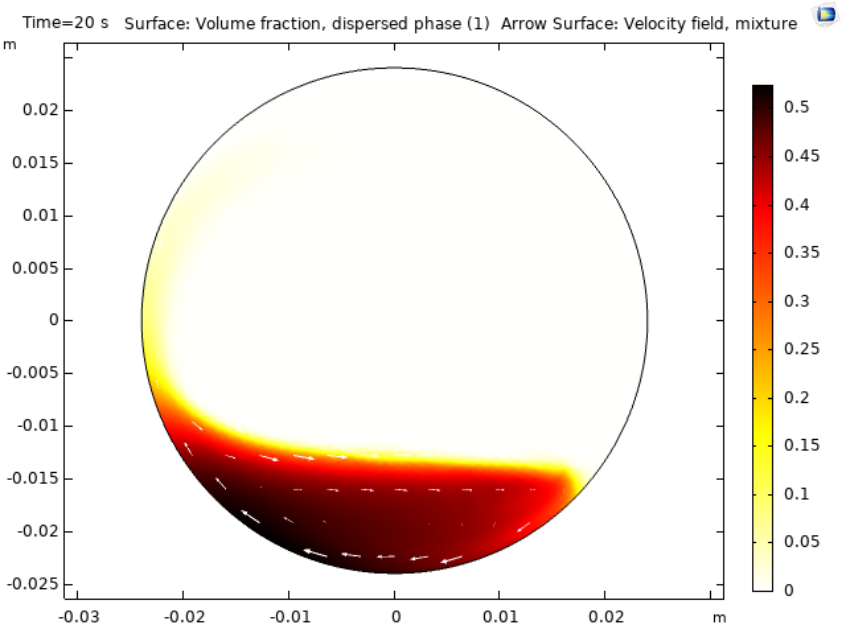

Figure 5.5.9: The flow regime of the bed in rolling mode with a filling degree of 0.23 with 40 RPM the white arrows showing the direction of the rotation.

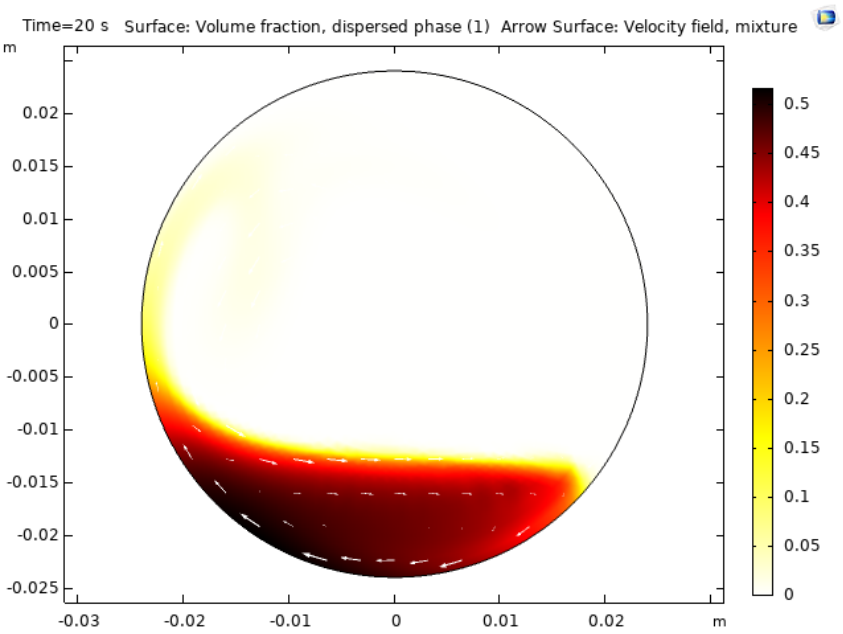

Figure 5.5.10: The flow regime of the bed in rolling mode with a filling degree of 0.23 with 45 RPM the white arrows showing the direction of the rotation.

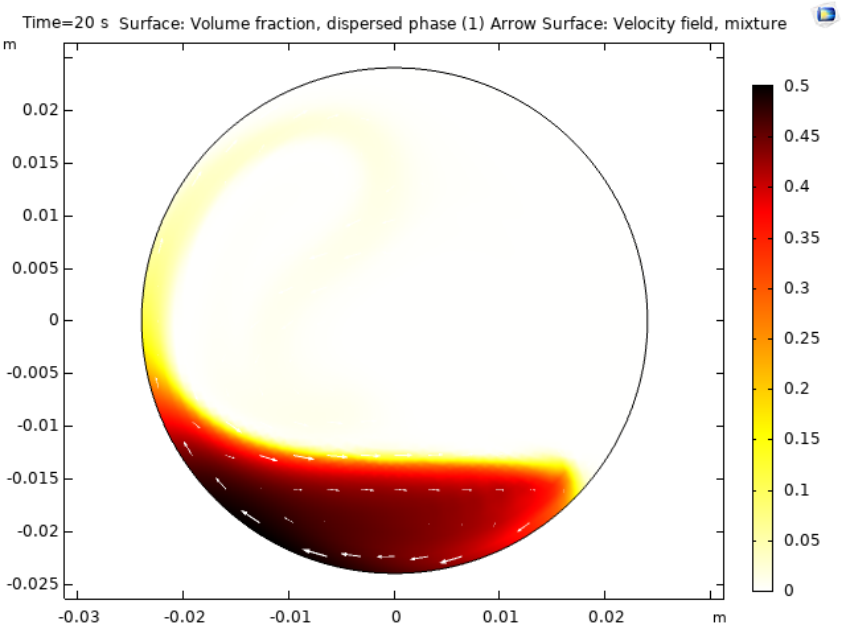

Figure 5.5.11: The flow regime of the bed in rolling mode with a filling degree of 0.23 with 50 RPM the white arrows showing the direction of the rotation.

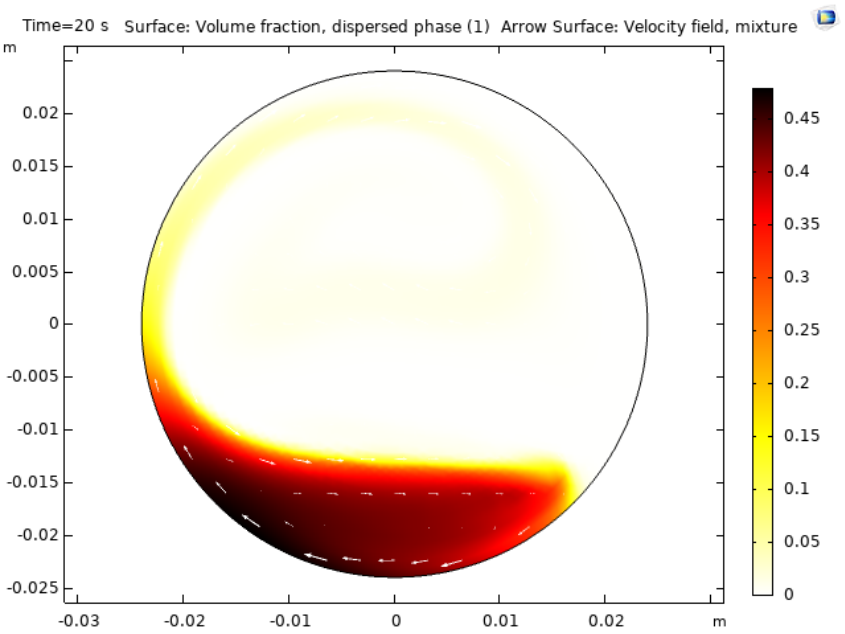

Figure 5.5.12: The flow regime of the bed in rolling mode with a filling degree of 0.23 with 60 RPM the white arrows showing the direction of the rotation.

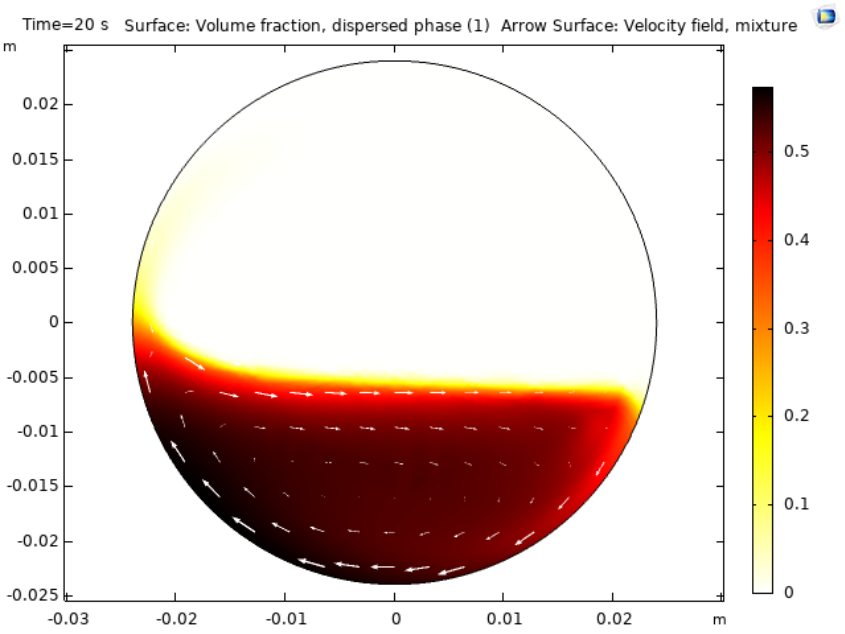

Figure 5.5.13: The flow regime of the bed in rolling mode with a filling degree of 0.3 with 35 RPM the white arrows showing the direction of the rotation.

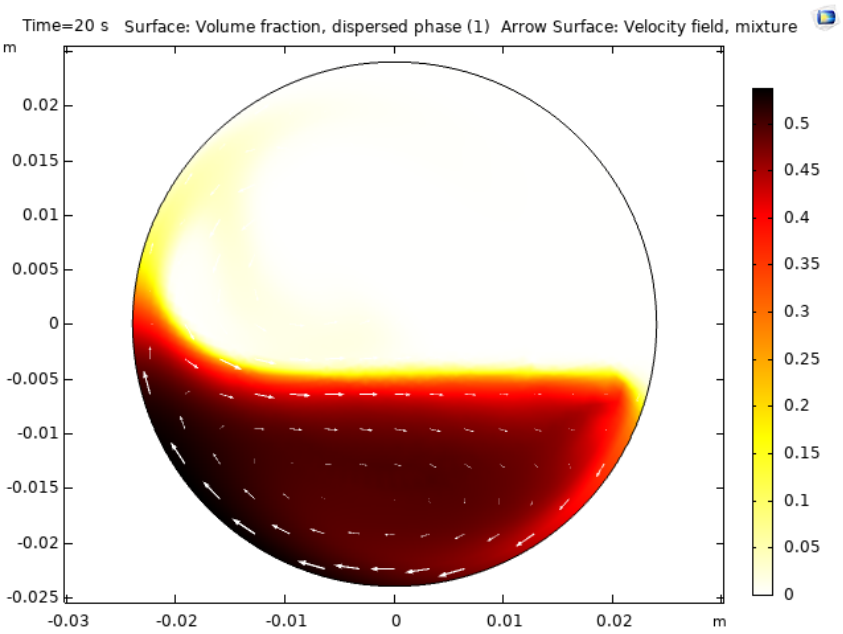

Figure 5.5.14: The flow regime of the bed in rolling mode with a filling degree of 0.3 with 55 RPM the white arrows showing the direction of the rotation.

5.5.4 Cascading, Cataracting and Centrifuging mode

For the remaining three modes, namely cascading, cataracting, and centrifuging the suspension model could not simulate the bed behaviour that was expected from figure 1.3.2. Instead, the results showed a flow regime of the bed similar to a mixer as seen in figures 5.5.15-5.5.19. The passive and active layer do not exist and instead the particles in the bed have now spread out in the mixer. The pattern that is seen in all of the figures show a higher concentration on one side of the wall than the other side. Also, at the top of the kiln, there is also less concentration than at the bottom. The reason for this is because the viscosity that is used changes with respect to the concentration. As the concentration is spread out due to the shearing, the viscosity becomes less which results in the viscous forces becoming less as seen in eq 2.2.1. This in turn affects the irreversible effect from the spatially varying viscosity. The latter get diminished to the point where it almost becomes negligible as seen in figure 5.5.20. Thus, the bed will spread out throughout the rotary kiln and the sedimentation flux will pull down the particles at the top which is why there is less particles on the right side of the wall than on the left side as seen in figure 5.5.21. More experimental results of this is shown in appendix E.

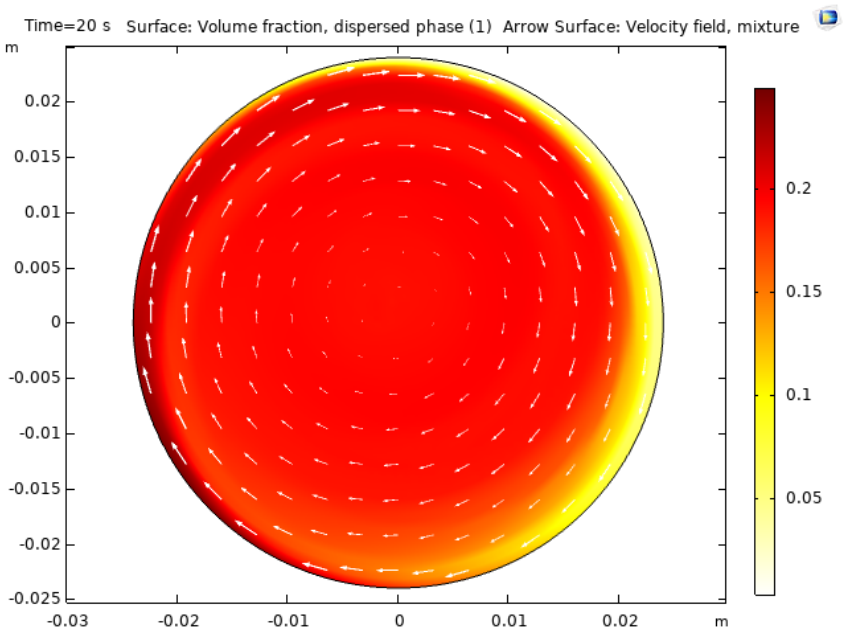

Figure 5.5.15: The flow regime of the bed in cascading mode with a filling degree of 0.3 with 150 RPM the white arrows showing the direction of the rotation.

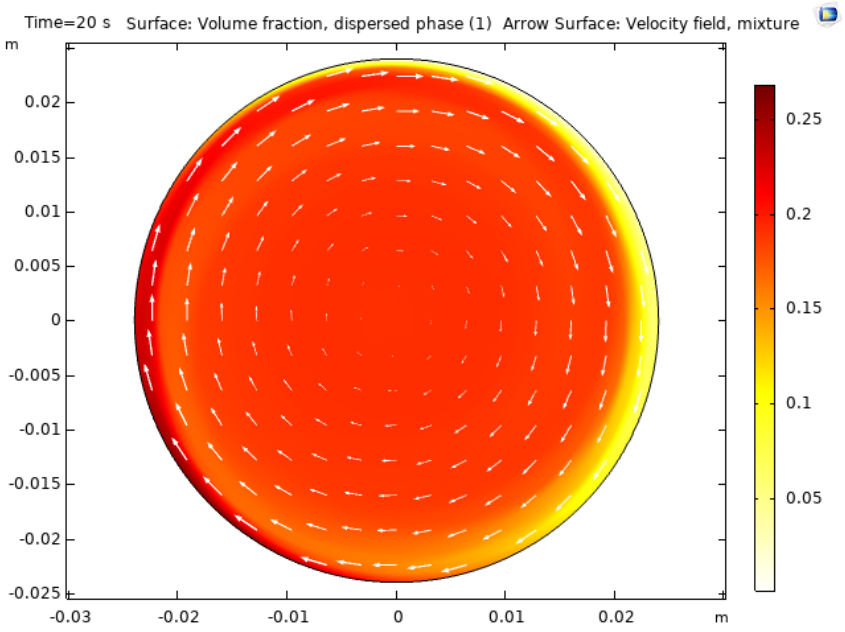

Figure 5.5.16: The flow regime of the bed in cascading mode with a filling degree of 0.3 with 170 RPM the white arrows showing the direction of the rotation.

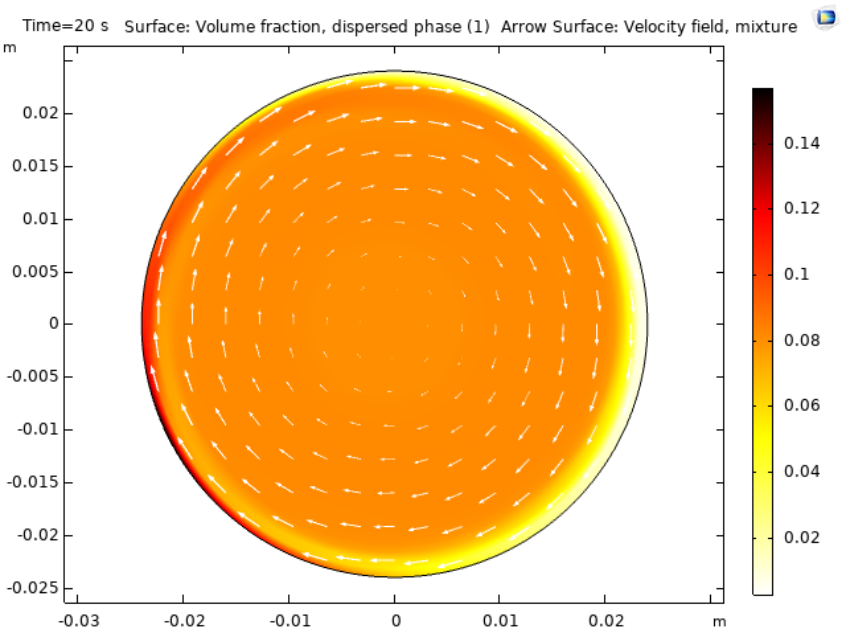

Figure 5.5.17: The flow regime in cataracting mode with a filling degree of 0.23 with 190 RPM the white arrows showing the direction of the rotation.

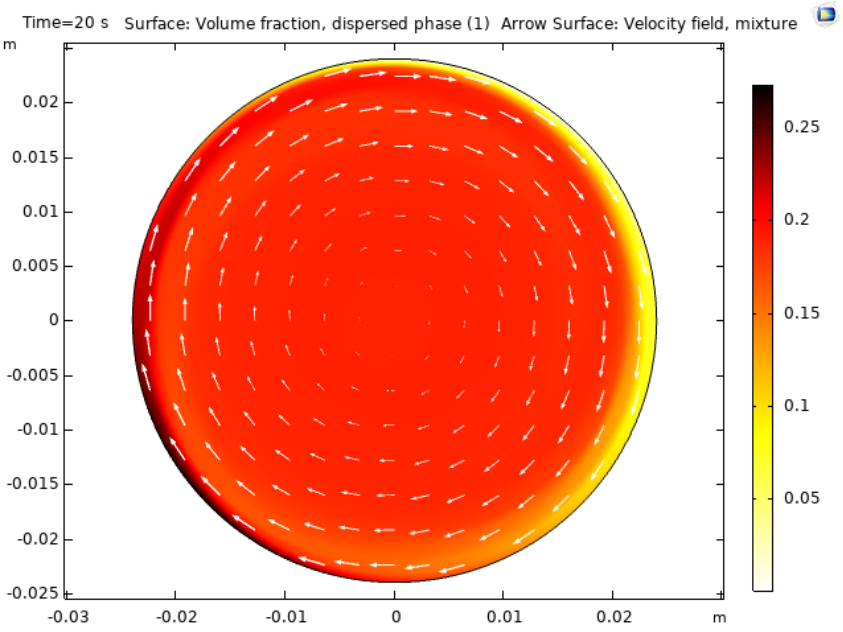

Figure 5.5.18: The flow regime in cataracting mode with a filling degree of 0.3 with 185 RPM the white arrows showing the direction of the rotation.

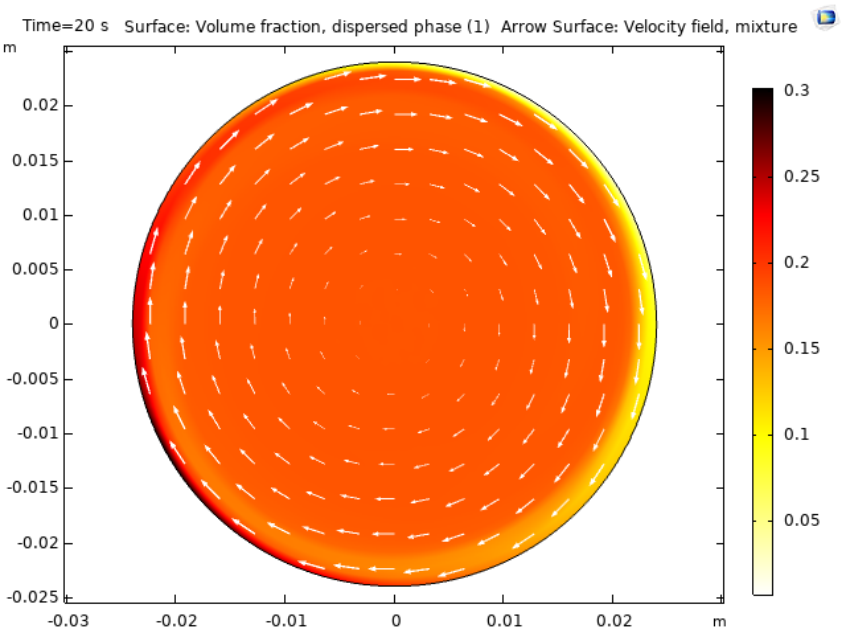

Figure 5.5.19: The flow regime in centrifuging mode with a filling degree of 0.3 with 250 RPM the white arrows showing the direction of the rotation.

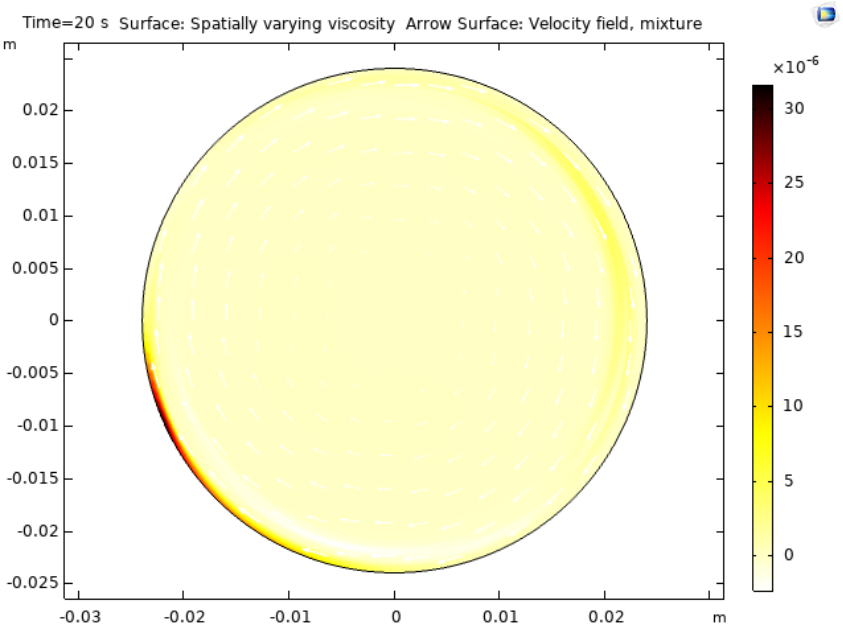

Figure 5.5.20: The spatially varying viscosity in the cascading mode with a filling degree of 0.23 and 200 RPM with white arrows showing the directions of the rotations.

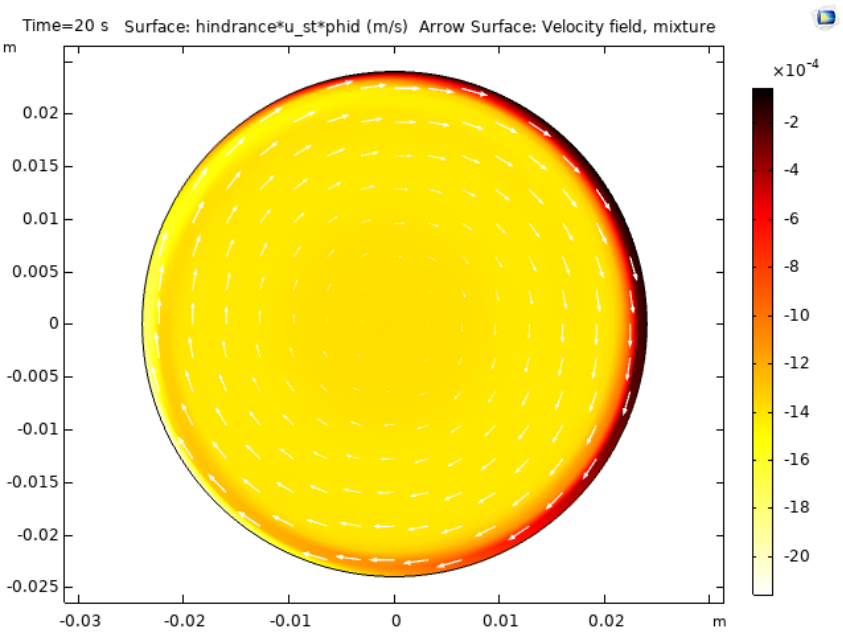

Figure 5.5.21: The sedimentation flux in the cascading mode with a filling degree of 0.23 and 200 RPM with white arrows showing the directions of the rotations.

5.6 Sensitivity analysis of temperature properties

The time evolutions of the minimum temperature of the solid bed particles in the rotary kiln is seen in figure 5.6.1 and 5.6.2. The two figures show the influence of the of thermal conductivity and specific heat capacity on the minimum temperature respectively. It is seen that as the thermal conductivity is increased, the time to reach a homogeneous thermal profile is faster which is expected as the material is able to absorb heat faster resulting in the temperature reaching the wall faster and the difference between the air and solid particles reducing. This indicates that the thermal conductivity plays a vital role for the heat absorption within the rotary kiln and having it be at least 15 (W/(m*K)) or higher to reach a homogeneous temperature profile around 5 seconds.

For the specific heat capacity, the thermal analysis shows as the solid heat capacity is varied the time to reach a homogeneous temperature profile does not change that much as the value of θ around 4 seconds is the same. This indicates that for the range of variation of 300 - 800 (J/(kg*K)), the difference of solid heat capacity is not that significant as they all reach a homogeneous temperature profile around the same time. Thus, it is shown that the variation of thermal conductivity has a more significant impact than the specific heat capacity.

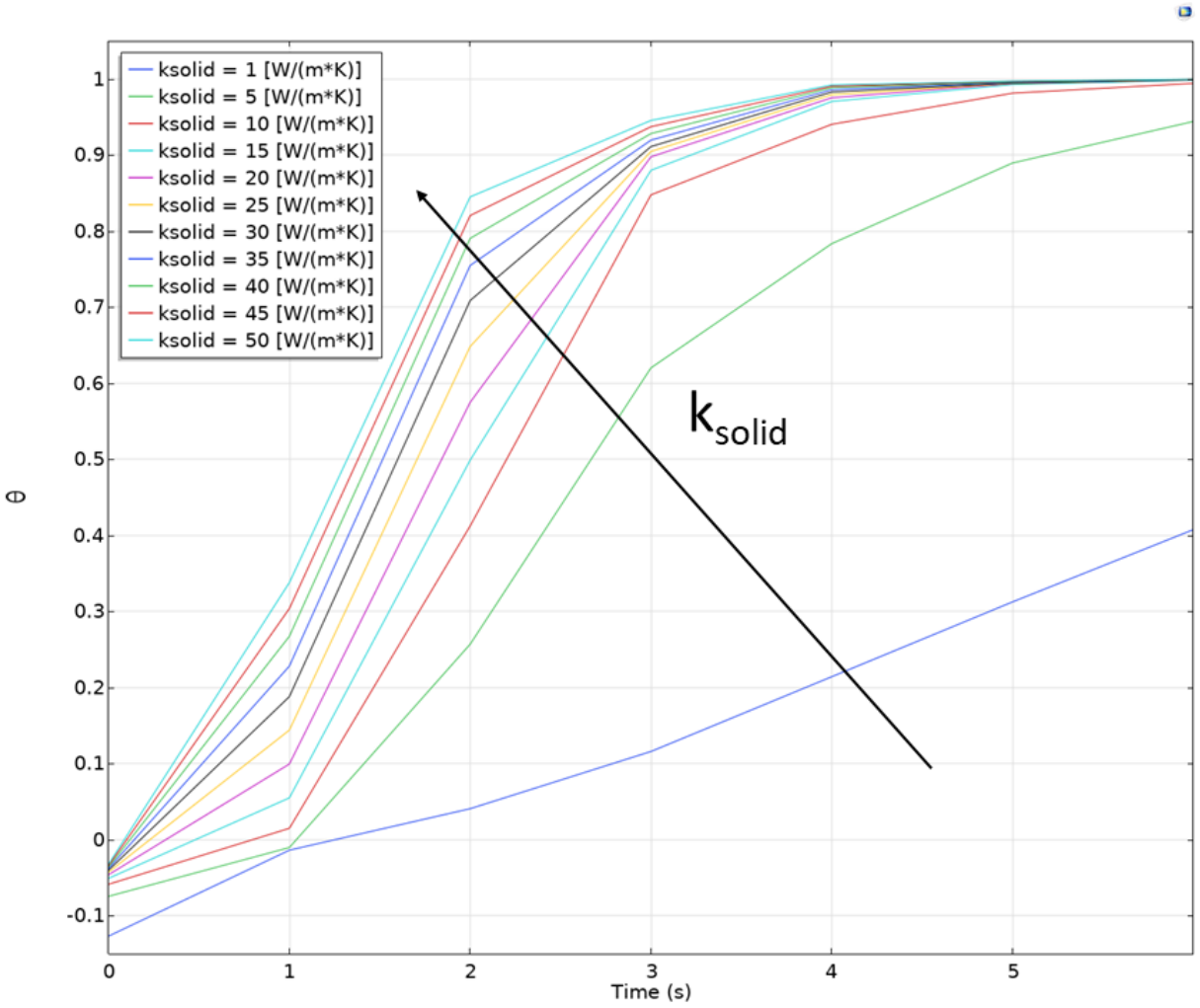

Figure 5.6.1: Sensitivity analysis of the solid thermal conductivity, k_s, varying from 1 - 50 (W/(m*K)) during rolling mode.

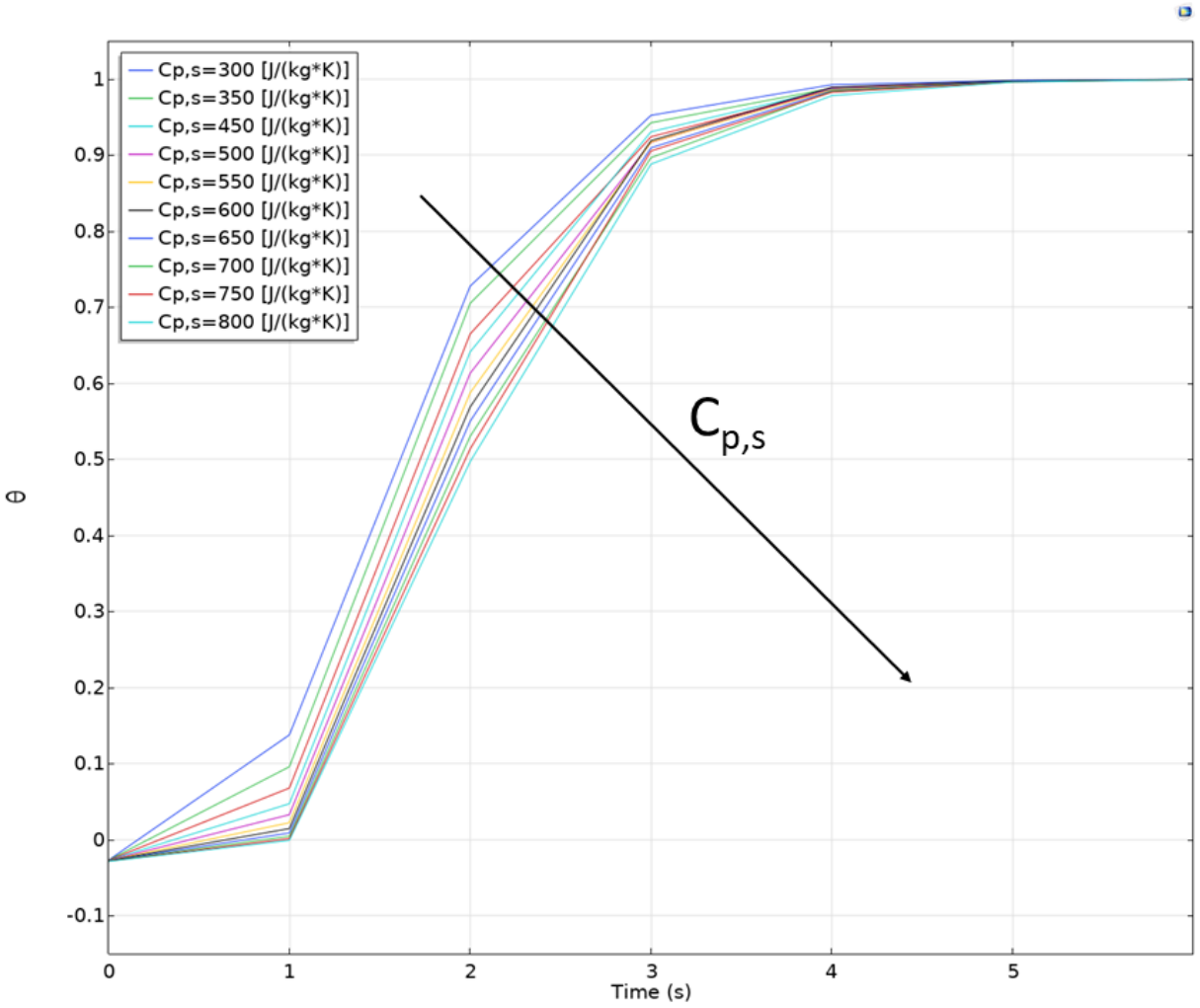

Figure 5.6.2: Sensitivity analysis of the solid specific heat capacity, $C_{p,s}$, varying from 300 - 800 (J/(kg*K)) during rolling mode.

Chapter 6

Conclusion and Future Work

6.1 Conclusion

The suspension model is an inexpensive model that is capable of simulating two phases as a single phase by introducing a particle flux model to represent the slip velocity for solid particles in the bed of a rotary kiln. Out of the six known different bed behaviours documented for a rotary kiln with respect to the Froude number and filling degree, the suspension model was capable of simulating the slipping mode accurately. For the remaining bed behaviour modes, namely slumping, rolling, cascading, cataracting, and centrifuging the model was not able to simulate what has been documented. The reason for this is due to the angle of repose being low resulting in the stickiness of the particles in the bed being low which is seen in the slumping mode as the particles did not reach an certain elevation and then suddenly drop. For the rolling mode, this phenomenon is also seen as the rolling mode behaved more as a cataracting mode due to the angle of repose being low and the viscous forces being low as well resulting in shearing having a greater effect than what is to be expected. The effect of shearing is seen most in the last three remaining bed behaviour flows (cascading, cataracting, and centrifuging) as the rotation speeds becomes too high shearing takes over resulting in a flow regime seen in mixers.

The heat analysis shows the impact of thermal conductivity and specific heat capacity of the solid on the temperature evolution in the rotary kiln. It was shown that for the specific heat capacity the variation from 300 - 800 (J/(kg*K)) did not impact the time to reach a homogeneous temperature profile. The variation in thermal conductivity however, was proven to have a more significant impact on the time to reach a homogeneous temperature profile in the range of 1 - 50 (W/(m*K)). Thus, it it is a more significant parameter that should be taken into

account when working with rotary kiln in this suspension model.

6.2 Future work

For future works, there are two main paths that can be chosen for describing the rotary kiln through a CFD perspective with a solid and gas phase. The first path is to continue working on the suspension model presented in this report and implementing another viscosity model such as the volume-average mixture model. This model is capable of accounting for the viscosity of both phases which may lead to a more accurate description of the known bed behaviour modes due to the viscous forces increasing. This would mean that the experimental coefficients would have to be investigated once again to fit the new model.

The other path is to simulate the solid and gas phase with the Euler-Euler method where each phase will instead have their own individual conservation equation for both mass and momentum transfers[28]. The amount of phases that are to be simulated is up to the user to decide, but normally the number is around 2 (usually the solid phase is represented as a mixture of solids and the gas by itself). The Euler-Euler method is usually seen being combined with the kinetic theory of granular flow (KTGF) method which introduces a new variable known as the granular temperature which represents the kinetic energy of the solids. The KTGF method is essentially the theory that will help calculate the viscous forces that are being applied on the solid particles. With these models coupled with one another, it is possible to simulate accurate bed behaviour diagrams. The impact of particle radius was investigated through the use of different different drag models [21][22][23]. However, it should be noted that the Euler-Euler method is already a computationally challenging method as each phase adds another set of boundary conditions. Also, the coupling of the KTGF method will result in more boundary conditions being applied making the system a challenge in itself to solve. Thus, the recommendation would be to first establish a computational environment for the Euler-Euler method using for the two phases gas and solid where the solid phase in a 2D cross section of a rotary kiln. Then, the implementation of the KTGF method should be performed for the establish model. Afterwards, the bed behaviour diagrams should be investigated to see if it can accurately describe the general modes that have been documented.

References

[1] Akwasi Boateng. *Rotray Kiln: transport phenomena and transport processes.* Butterworth-Heinemann, 2008, pp. 3–5. ISBN: 978-0-7506-7877-3.

[2] Michael David Heydenrych. "Modelling of Rotary Kilns". In: (), pp. 1–6.

[3] H Henein, JK Brimacombe, and AP Watkinson. "Experimental study of transverse bed motion in rotary kilns". In: *Metallurgical transactions B* 14.2 (1983), pp. 191–205.

[4] Jeff Susantha Dissanayake, H.D.s.s Karunarathne, Joachim Lundberg, and Lars-André Tokheim. "CFD Study of Particle Flow Patterns in a Rotating Cylinder Applying OpenFOAM and Fluent". In: Sept. 2017, pp. 137–143. DOI: 10.3384/ecp17138137.

[5] Akwasi Boateng. *Rotray Kiln: transport phenomena and transport processes.* Butterworth-Heinemann, 2008, pp. 156–157. ISBN: 978-0-7506-7877-3.

[6] David Leighton and Andreas Acrivos. "The shear-induced migration of particles in concentrated suspensions". In: *Journal of Fluid Mechanics* 181 (1987), pp. 415–439.

[7] Ronald J Phillips, Robert C Armstrong, Robert A Brown, Alan L Graham, and James R Abbott. "A constitutive equation for concentrated suspensions that accounts for shear-induced particle migration". In: *Physics of Fluids A: Fluid Dynamics* 4.1 (1992), pp. 30–40.

[8] K Zhang and A Acrivos. "Viscous resuspension in fully developed laminar pipe flows". In: *International journal of multiphase flow* 20.3 (1994), pp. 579–591.

[9] COMSOL. *5.5 CFD Module User's Guide,* 2019, pp. 474–477.

[10] MS Manju and S Savithri. "Three dimensional CFD simulation of pneumatic coal injection in a direct reduction rotary kiln". In: *Fuel* 102 (2012), pp. 54–64.

[11] Peter J Witt, Matthew D Sinnott, Paul W Cleary, and M Philip Schwarz. “A hierarchical simulation methodology for rotary kilns including granular flow and heat transfer”. In: *Minerals Engineering* 119 (2018), pp. 244–262.

[12] Gajendra Kumar Gaurav and Shabina Khanam. “Analysis of temperature profile and% metallization in rotary kiln of sponge iron process through CFD”. In: *Journal of the Taiwan Institute of Chemical Engineers* 63 (2016), pp. 473–481.

[13] Gajendra Kumar Gaurav and Shabina Khanam. “Computational fluid dynamics analysis of sponge iron rotary kiln”. In: *Case Studies in Thermal Engineering* 9 (2017), pp. 14–27.

[14] Hassan Fawzy Mohamed Elattar et al. “Flame simulation in rotary kilns using computational fluid dynamics”. In: (2011).

[15] Matthäus U. Bäbler. *Transport Phenomena Advanced Course*. 2019, pp. 53–58.

[16] Gui-Rong Liu and Siu Sin Quek. *The finite element method: a practical course*. Butterworth-Heinemann, 2013, pp. 1–11.

[17] Samuel R Subia, Marc S Ingber, Lisa A Mondy, Steve A Altobelli, and Alan L Graham. “Modelling of concentrated suspensions using a continuum constitutive equation”. In: *Journal of Fluid Mechanics* 373 (1998), pp. 193–219.

[18] Rekha Rao, Lisa Mondy, Amy Sun, and Steve Altobelli. “A numerical and experimental study of batch sedimentation and viscous resuspension”. In: *International journal for numerical methods in fluids* 39.6 (2002), pp. 465–483.

[19] Seyyed Hossein Hosseini, Goodarz Ahmadi, and Martin Olazar. “CFD simulation of cylindrical spouted beds by the kinetic theory of granular flow”. In: *Powder technology* 246 (2013), pp. 303–316.

[20] Robin Schmidt and Petr A Nikrityuk. “Numerical simulation of the transient temperature distribution inside moving particles”. In: *The Canadian Journal of Chemical Engineering* 90.2 (2012), pp. 246–262.

[21] Sumudu S Karunarathne and Lars-André Tokheim. “Comparison of the influence of drag models in CFD simulation of particle mixing and segregation in a rotating cylinder”. In: (2017).

[22] Sumudu S Karunarathne, Chameera K Jayarathna, and Lars-Andre Tokheim. “Mixing and segregation in a rotating cylinder: CFD simulation and experimental study”. In: *International Journal of Modeling and Optimization* 7.1 (2017), p. 1.

[23] Sumudu Karunarathne, Chameera Jayarathna, and Lars-Andre Tokheim. "Impact of particle diameter, particle density and degree of filling on the flow behavior of solid particle mixtures in a rotating drum". In: *Proceedings of The 9th EUROSIM Congress on Modelling and Simulation, EUROSIM 2016, The 57th SIMS Conference on Simulation and Modelling SIMS 2016*. 142. Linköping University Electronic Press. 2018, pp. 1013–1018.

[24] Rashid Jamshidi, Jurriaan JJ Gillissen, Panagiota Angeli, and Luca Mazzei. "Roles of solid effective stress and fluid-particle interaction force in modeling shear-induced particle migration in non-Brownian suspensions". In: *Physical Review Fluids* 6.1 (2021), p. 014301.

[25] Marko Korhonen, Kristian Wallgren, Antti Puisto, Mikko Alava, and Ville Vuorinen. "Shear localization in large amplitude oscillatory shear (LAOS) flows of particulate suspensions". In: *Physical Review Fluids* 6.3 (2021), p. 033302.

[26] Engineers Edge. *Thermal Conductivity of Gases Chart*. 2021. URL: https://www.engineersedge.com/heattransfer/thermal-conductivity-gases.htm (visited on 06/16/2021).

[27] Engineering Toolbox. *Oxygen Gas - Specific Heat*. 2005. URL: https://www.engineeringtoolbox.com/oxygen-d978.html (visited on 06/16/2020).

[28] CKK Lun and SB Savage. "A simple kinetic theory for granular flow of rough, inelastic, spherical particles". In: (1987).

Chapter A

Appendix

Here the remaining experiments conducted will be presented here for further proof of the statements made.

A Experimental parameters

As mentioned earlier, the variation of experimental parameters that was conducted will be illustrated here to further prove that the value K_c and K_μ was chosen correctly.

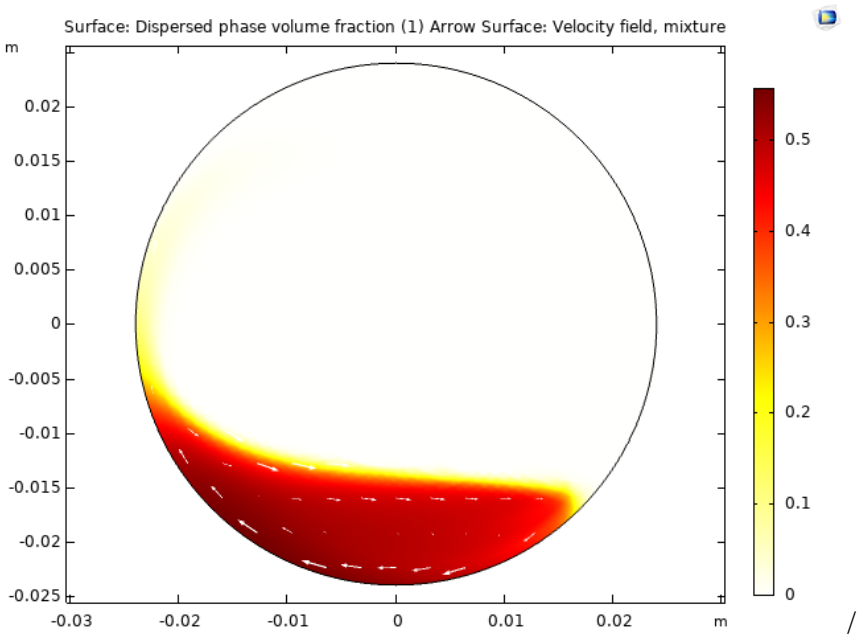

Figure A.1: The flow regime of the bed in rolling mode with $K_c = K_\mu = 2$ with the white arrows showing the direction of the rotation.

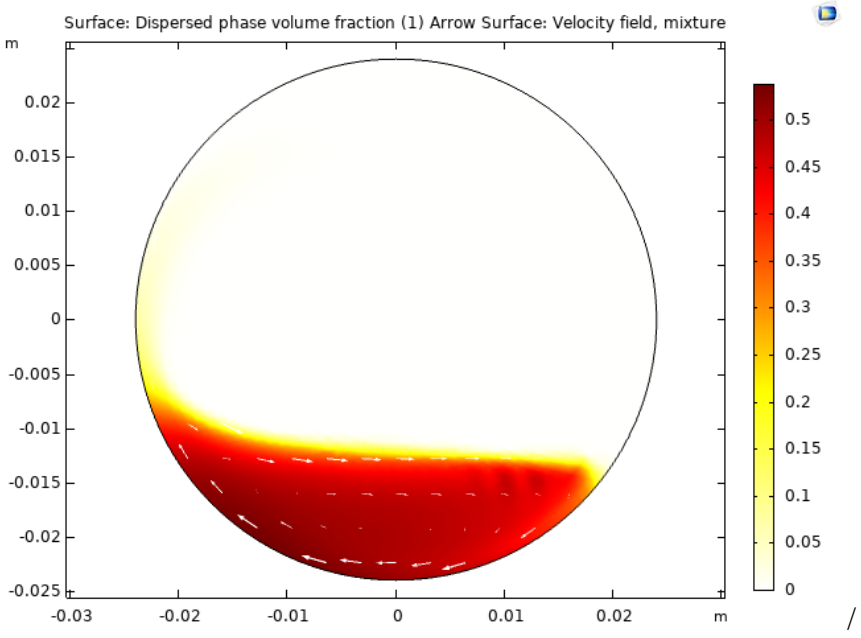

Figure A.2: The flow regime of the bed in rolling mode with $K_c = K_\mu = 5$ with the white arrows showing the direction of the rotation.

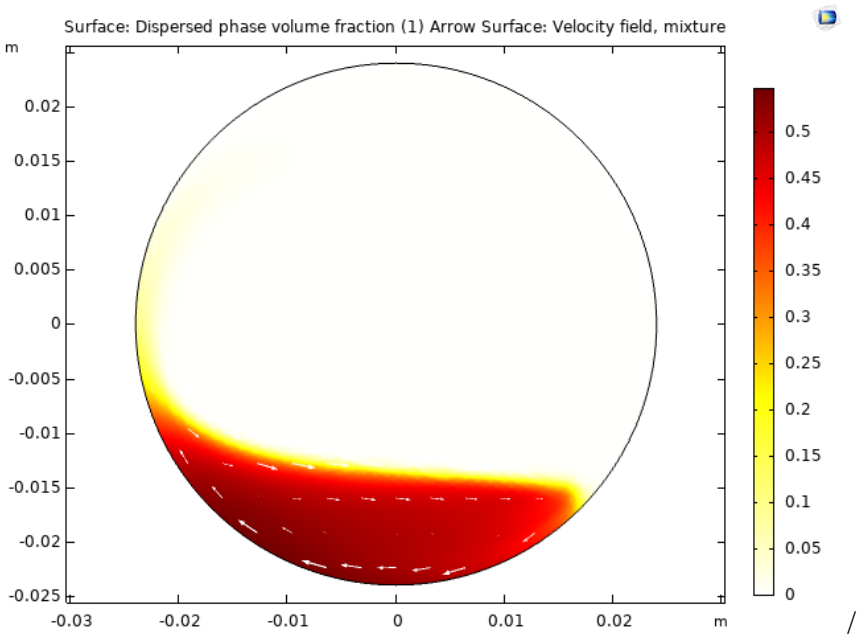

Figure A.3: The flow regime of the bed in rolling mode with K_c = 2 and K_μ = 3 with the white arrows showing the direction of the rotation.

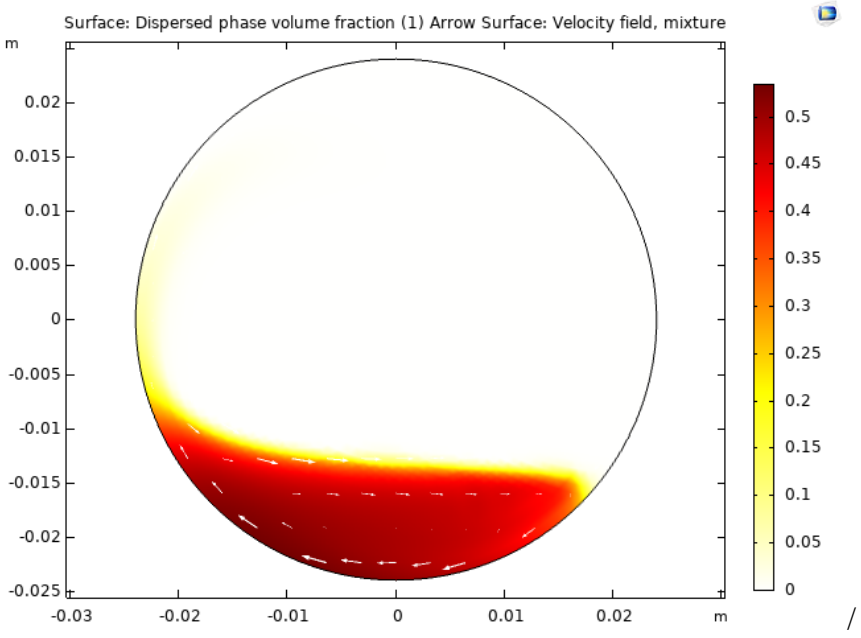

Figure A.4: The flow regime of the bed in rolling mode with K_c = 3.1 and K_μ = 4.1 with the white arrows showing the direction of the rotation.

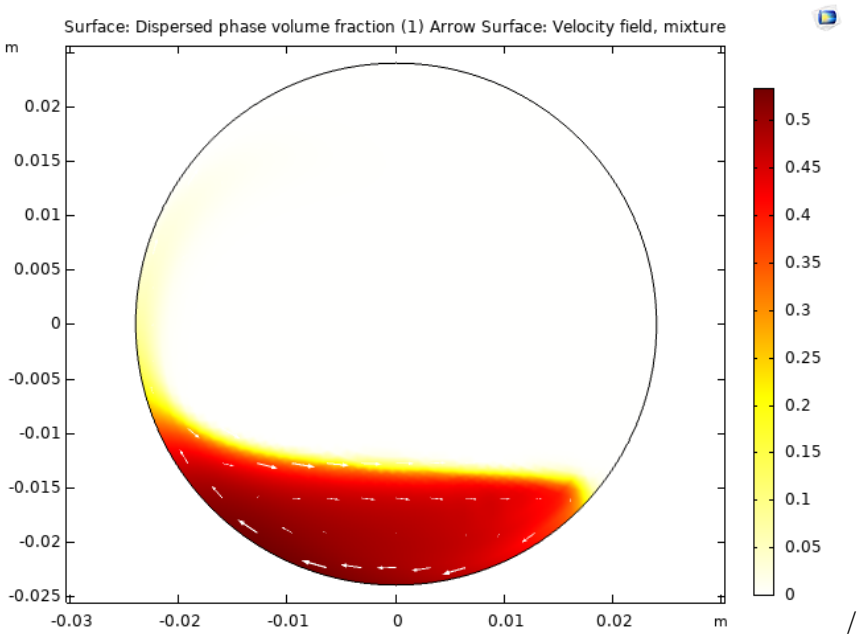

Figure A.5: The flow regime of the bed in rolling mode with K_c = 3.2 and K_μ = 4.2 with the white arrows showing the direction of the rotation.

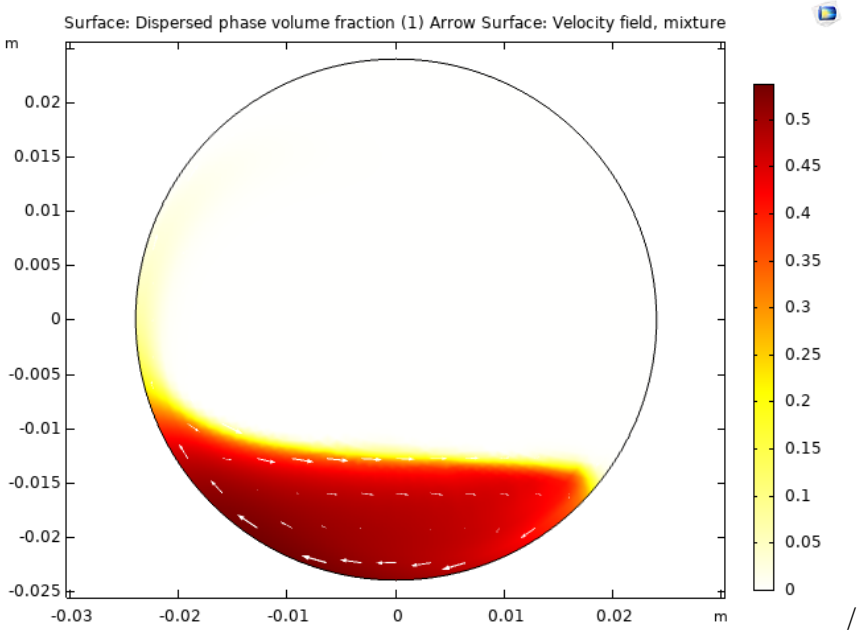

Figure A.6: The flow regime of the bed in rolling mode with K_c = 3.3 and K_μ = 4.3 with the white arrows showing the direction of the rotation.

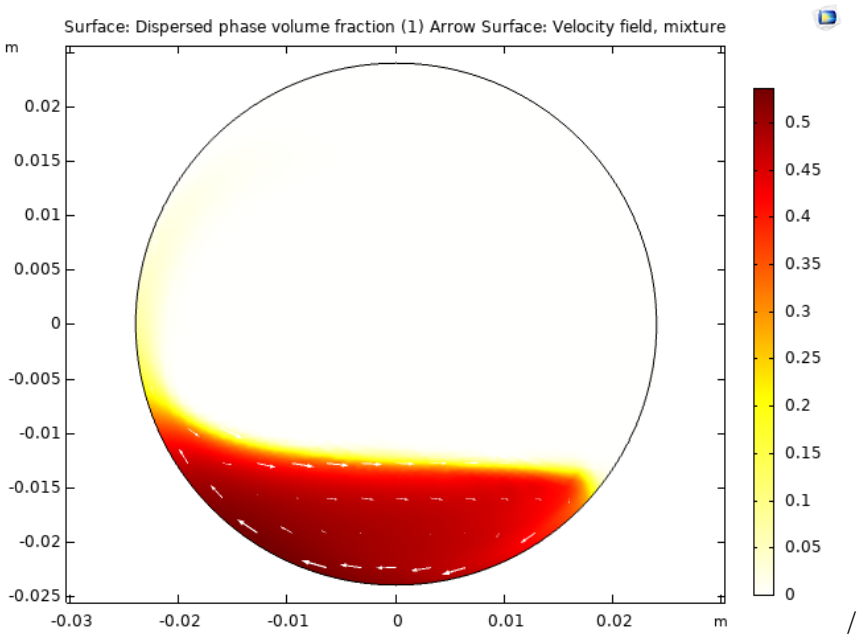

Figure A.7: The flow regime of the bed in rolling mode with K_c = 3.4 and K_μ = 4.4 with the white arrows showing the direction of the rotation.

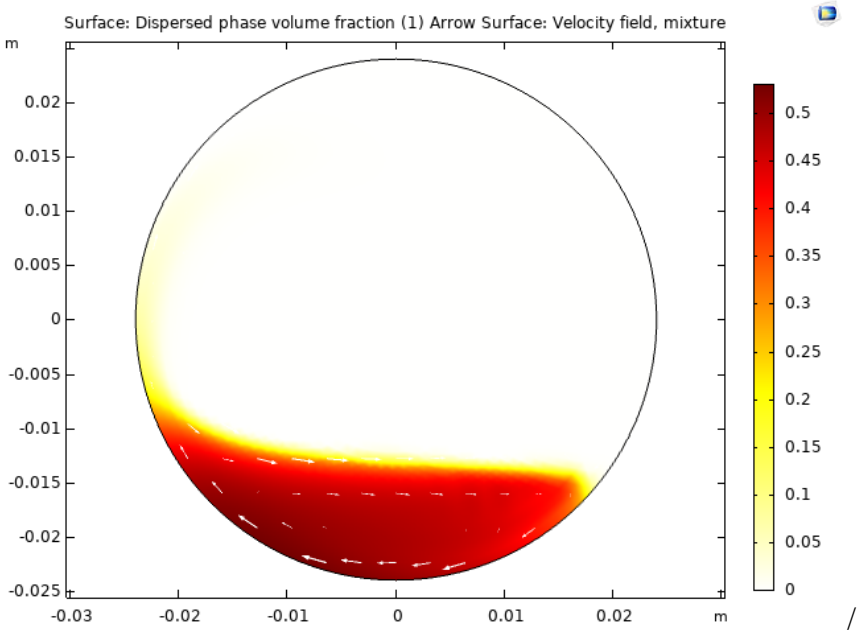

Figure A.8: The flow regime of the bed in rolling mode with K_c = 3.5 and K_μ = 4.5 with the white arrows showing the direction of the rotation.

B Solid particle radius

In this section, it is seen that the variation differences between 0.6 mm to 0.8 mm are not that significant leading to the conclusion mentioned earlier that a minimum radius of 0.4 mm is sufficient to increase the viscous forces.

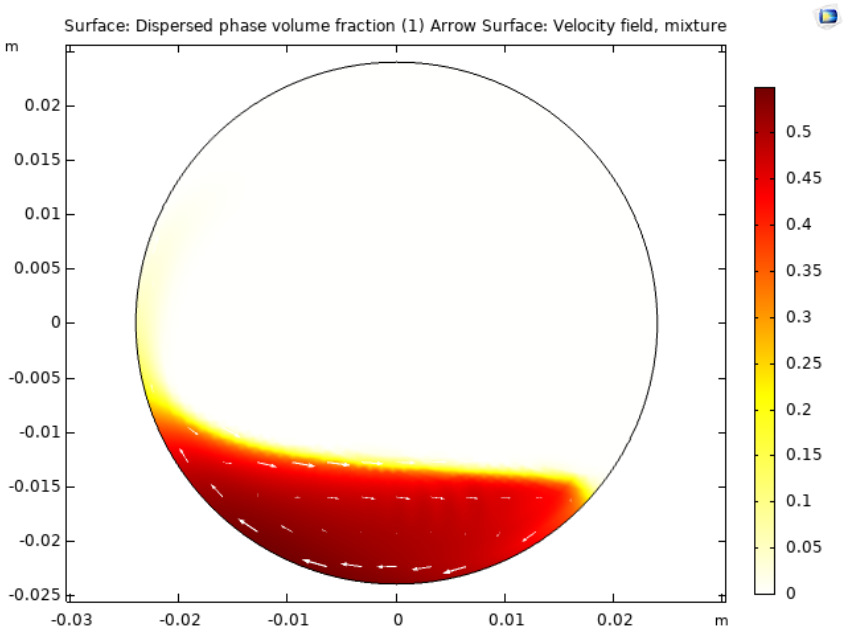

Figure B.1: The flow regime of the bed in rolling mode with a solid particle radius of 0.6 mm with the white arrows showing the direction of the rotation.

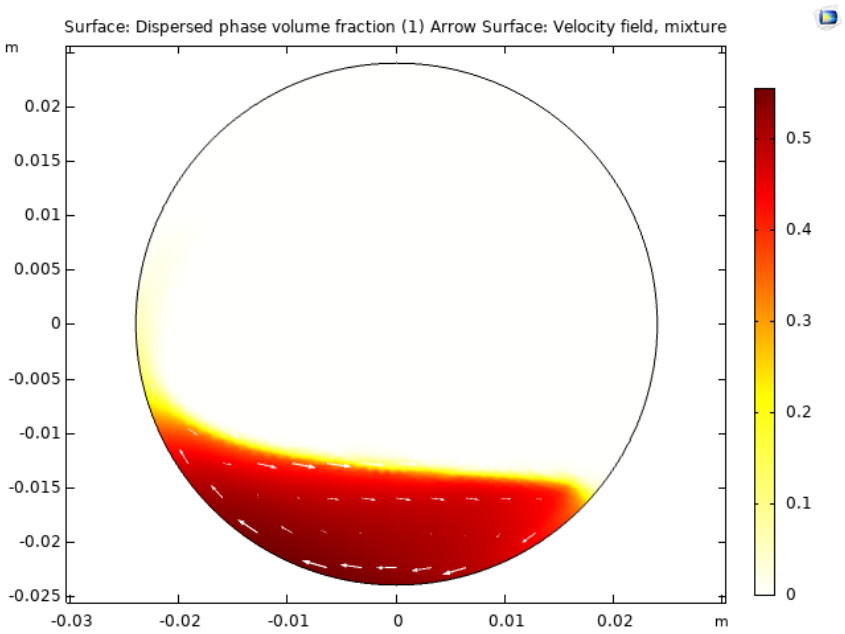

Figure B.2: The flow regime of the bed in rolling mode with a solid particle radius of 0.7 mm with the white arrows showing the direction of the rotation.

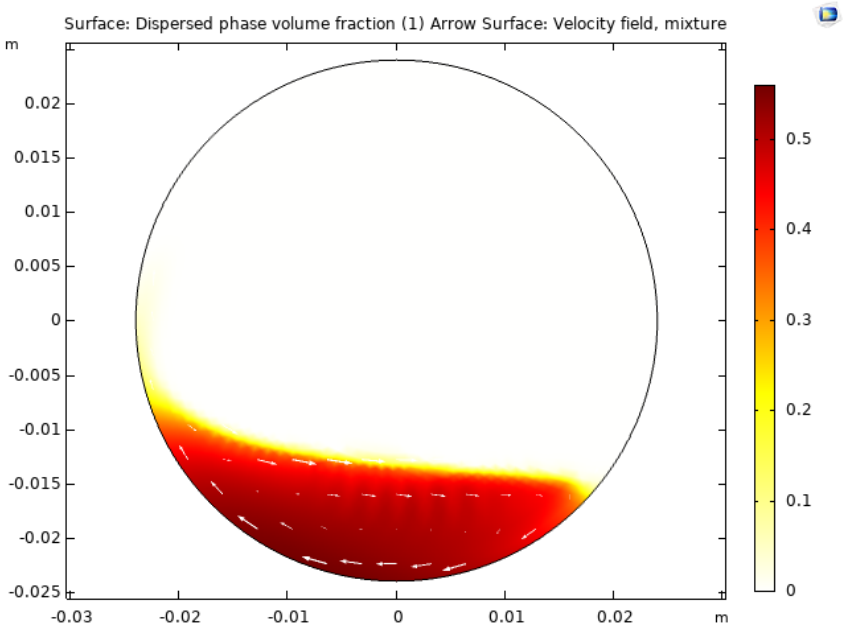

Figure B.3: The flow regime of the bed in rolling mode with a solid particle radius of 0.8 mm with the white arrows showing the direction of the rotation.

C Particle density

In this section, it is seen that the solid density between 2500 and 2750 kg/m^3 are shown. It is seen that nothing there is no significant change in the flow regime as the density is increased further on from this point.

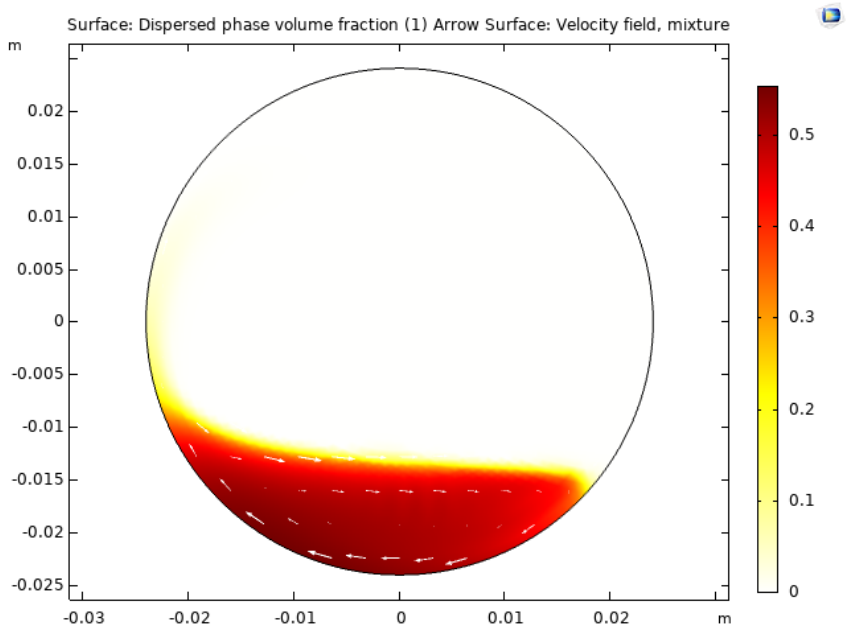

Figure C.1: Then flow regime in rolling mode with a particle density of 2500 kg/m^3 with the white arrows showing the direction of rotation.

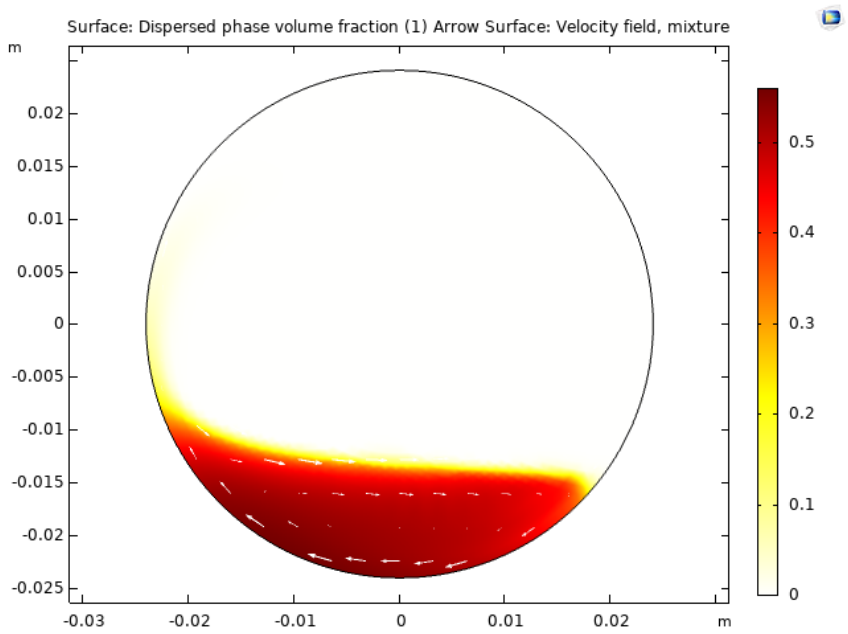

Figure C.2: The flow regime in rolling mode with a particle density of 2750 kg/m^3 with the white arrows showing the direction of rotation.

D Rolling mode

In this section the remaining results from the rolling mode at different filling degrees is seen. It is shown that even though the rotation and filling degree changed, similar bed behaviour was seen as the particles still experiences free falling after a certain elevation was reached resembling that of a cataracting mode.

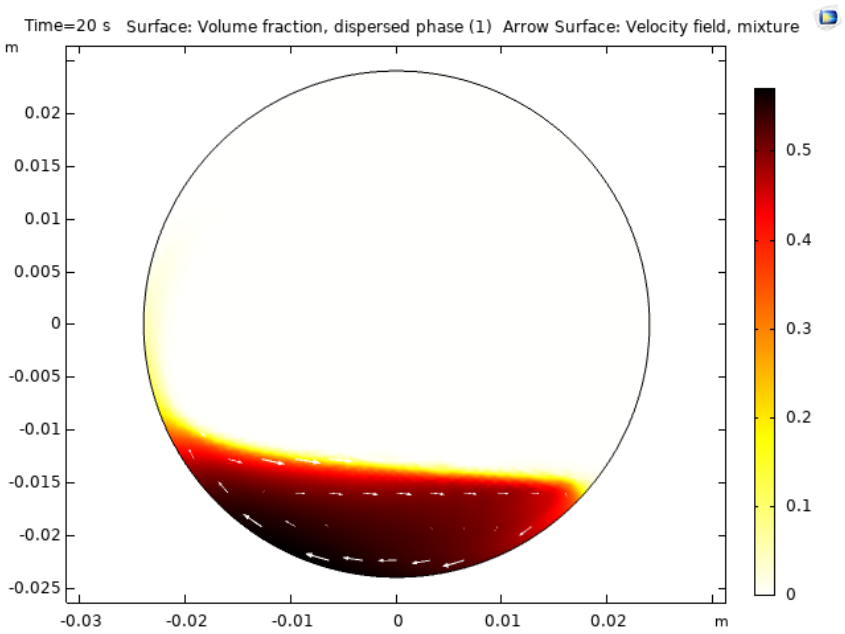

Figure D.1: The flow regime of the bed in rolling mode with a filling degree of 0.23 with 20 RPM the white arrows showing the direction of the rotation.

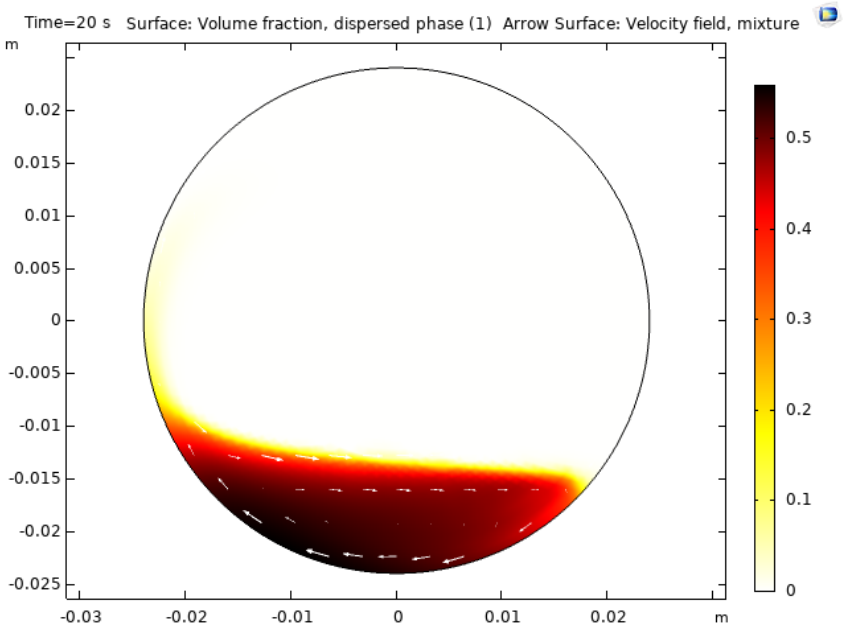

Figure D.2: The flow regime of the bed in rolling mode with a filling degree of 0.23 with 25 RPM the white arrows showing the direction of the rotation.

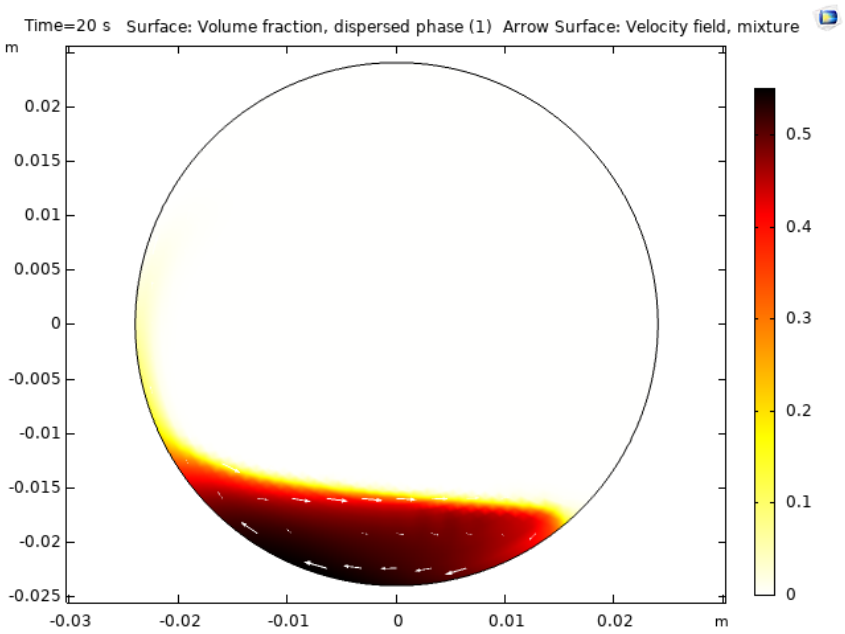

Figure D.3: The flow regime of the bedin rolling mode with a filling degree of 0.1 with 20 RPM the white arrows showing the direction of the rotation.

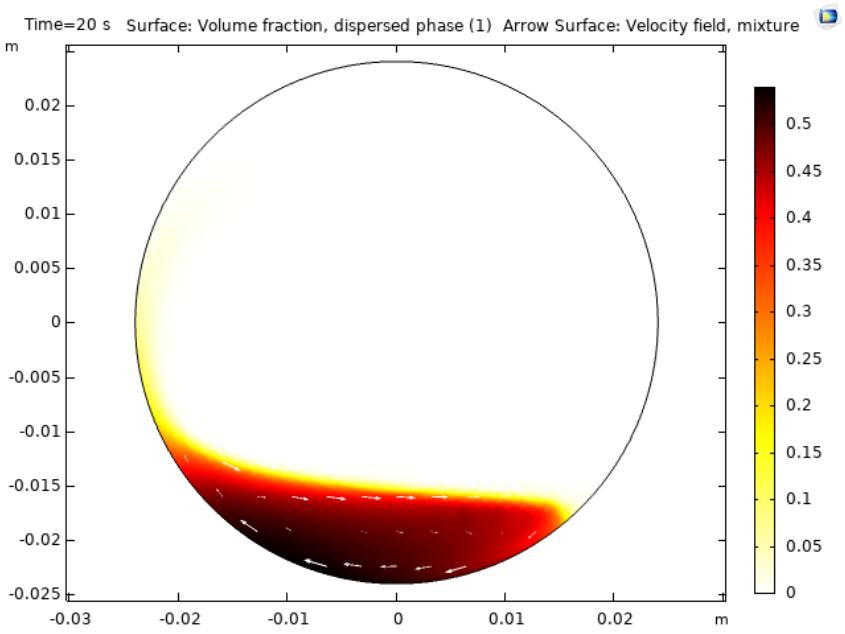

Figure D.4: The flow regime of the bed in rolling mode with a filling degree of 0.1 with 25 RPM the white arrows showing the direction of the rotation.

E Cetrifuging mode

In this section, the remaining results from the centrifuging mode are shown. More experiments were conducted on this mode as it was to be studied if the rotation speed itself if increased could result in the solid particles sticking to the wall as documented. It is seen that even though the filling degree and rotation speed varies the results are similar when it comes to the flow regime of the bed as it spreads out throughout the kiln.

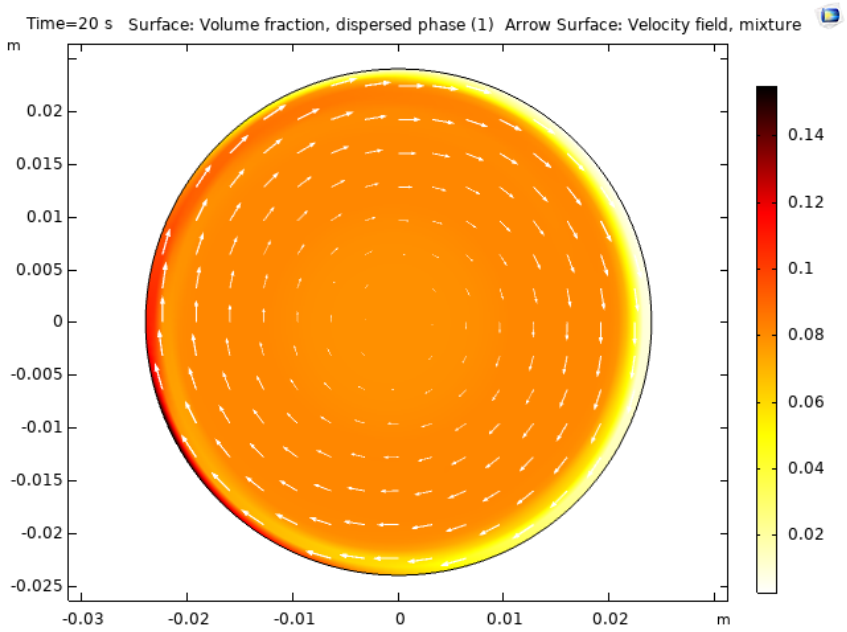

Figure E.1: The flow regime in centrifuging mode with a filling degree of 0.23 with 200 RPM the white arrows showing the direction of the rotation.

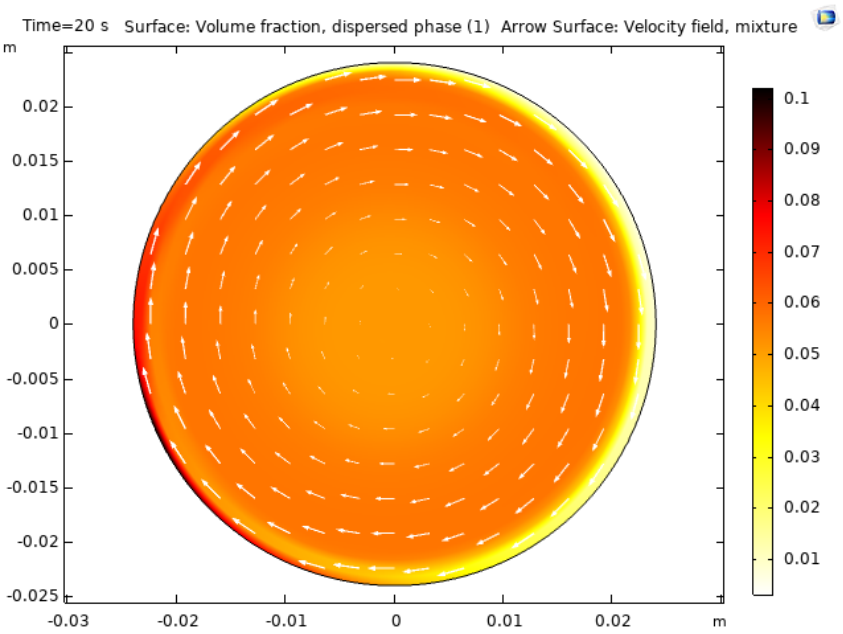

Figure E.2: The flow regime in centrifuging mode with a filling degree of 0.1 with 250 RPM the white arrows showing the direction of the rotation.